Theor Chem Account (2008) 119:191–210
DOI 10.1007/s00214-007-0361-z

REGULAR ARTICLE

Role of hydration in determining the structure and vibrational spectra of L-alanine and *N*-acetyl L-alanine *N′*-methylamide in aqueous solution: a combined theoretical and experimental approach

K. J. Jalkanen · I. M. Degtyarenko · R. M. Nieminen · X. Cao · L. A. Nafie · F. Zhu · L. D. Barron

Received: 14 March 2007 / Accepted: 14 May 2007 / Published online: 9 August 2007

Abstract In this work we have utilized recent density functional theory Born-Oppenheimer molecular dynamics simulations to determine the first principles locations of the water molecules in the first solvation shell which are responsible for stabilizing the zwitterionic structure of L-alanine. Previous works have used chemical intuition or classical molecular dynamics simulations to position the water molecules. In addition, a complete shell of water molecules was not previously used, only the water molecules which were thought to be strongly interacting (H-bonded) with the zwitterionic species. In a previous work by Tajkhorshid et al. (J Phys Chem B 102:5899) the L-alanine zwitterion was stabilized by 4 water molecules, and a subsequent work by Frimand et al. (Chem Phys 255:165) the number was increased to 9 water molecules. Here we found that 20 water molecules are necessary to fully encapsulate the zwitterionic species when the molecule is embedded within a droplet of water, while 11 water molecules are necessary to encapsulate the polar region with the methyl group exposed to the surface, where it migrates during the MD simulation. Here we present our vibrational absorption, vibrational circular dichroism and Raman and Raman optical activity simulations, which we compare to the previous simulations and experimental results. In addition, we report new VA, VCD, Raman and ROA measurements for L-alanine in aqueous solution with the latest commercially available FTIR VA/VCD instrument (Biotools, Jupiter, FL, USA) and Raman/ROA instrument (Biotools). The signal to noise of the spectra of L-alanine measured with these new instruments is significantly better than the previously reported spectra. Finally we reinvestigate the causes for the stability of the P_π structure of the alanine dipeptide, also called *N*-acetyl-L-alanine *N′*-methylamide, in aqueous solution. Previously we utilized the B3LYP/6-31G* + Onsager continuum level of theory to investigate the stability of the NALANMA4WC Han et al. (J Phys Chem B 102:2587) Here we use the B3PW91 and B3LYP hybrid exchange correlation functionals, the aug-cc-pVDZ basis set and the PCM and CPCM (COSMO) continuum solvent models, in addition to the Onsager and no continuum solvent model. Here by the comparison of the VA, VCD, Raman and ROA spectra we can confirm the stability of the NALANMA4WC due to the strong hydrogen bonding between the

Festschift in Honor of Philip J. Stephens' 65th Birthday.

During the proof stage of this article a very relevant article has been published by M. Losada and Y. Xu titled "Chirality transfer through hydrogen-bonding: Experimental and ab initio analyses of vibrational circular dichroism spectra of methyl lactate in water" in Phys Chem Chem Phys 2007, 9: 3127–3135. In that work they confirm that the effects of water are seen in the VCD spectra and hence it is fundamental to include explicit water molecules in modeling studies of the vibrational spectra of biomolecules in aqueous solution.

K. J. Jalkanen (✉)
Nanochemistry Research Institute, Department of Applied Chemistry, Curtin University of Technology, GPO Box U1987, Perth, WA 6845, Australia
e-mail: jalkanen@ivec.org

I. M. Degtyarenko · R. M. Nieminen
Laboratory of Physics, Helsinki University of Technology, P.O. Box 1100, 02015 HUT, Espoo, Finland
e-mail: imd@fyslab.hut.fi

R. M. Nieminen
e-mail: Risto.Nieminen@hut.fi

X. Cao · L. A. Nafie
Department of Chemistry, Syracuse University, Syracuse, NY, USA
e-mail: lnafie@syr.edu

F. Zhu · L. D. Barron
Department of Chemistry, Glasgow University, Glasgow G12 8QQ, UK
e-mail: laurence@chem.gla.ac.uk

four water molecules and the peptide polar groups. Hence we advocate the use of explicit water molecules and continuum solvent treatment for all future spectral simulations of amino acids, peptides and proteins in aqueous solution, as even the structure (conformer) present cannot always be found without this level of theory.

1 Introduction

Methods which can be used to determine the structure of biomolecules in native and non-native conditions are necessary to be able to understand not only the interactions responsible for structural stability, but also to determine and understand their function [1–3]. X-ray and neutron diffraction methods are the methods of choice for biomolecules for which one can crystallize [4,5]. The assumption is that the conditions one uses to get the molecules to crystallize do not affect the structure, that is, the structure of the molecule in the crystal is the same as that in its functionally active state. This may indeed be the case for large proteins, but it is not obviously the case for small flexible molecules [6]. Additionally, nuclear magnetic resonance (NMR) methods have recently been used to supplement the diffraction methods, though in general the method only works for biomolecules which are in the folded state. This is because the NMR methods are based on the nuclear Overhauser effect (NOE), that is, the NOE signals occur only when two protons are close in distance. This is due to the signal strength being dependent on the distance to the negative 6th power. For extended or unfolded proteins, one normally does not have enough NOEs distant constraints to uniquely determine the structure. Hence alternative methods are required. Additionally one would like to be able to follow the conformational changes in the structures as a function of solvent polarity, addition of denaturing agents, changes in pH and addition of ligands [7]. Normal and chiral infrared (vibrational), Raman and electronic spectroscopies are very structure sensitive probes, and many changes have been observed in these spectra as a function of the solvent polarity, pH, phase and temperature [8–19]. The problem has been to date, interpretation of the changes in the spectra. Finally some workers have attempted to understand the biological properties of L-alanine (LA) and *N*-acetyl L-alanine *N*′-methylamide (NALANMA) by gas phase or isolated state simulations, but the species (LA) and conformer (NALANMA) have been shown to be fundamentally different [3,20–23].

In addition to using spectroscopic measurements to monitor changes due to solvents, Baker and coworkers have also investigated the redox potentials [24]. The redox potentials are shown to be a function of the solvent polarity and hydrogen bonding ability. For biochemical catalysis and function, is it important to not only understand the structural and vibrational properties, but also the electronic properties: oxidation and reduction potentials and how they can be tuned by neighboring residues and the protein, solvent and/or membrane environment.

Vibrational spectroscopic measurements have additionally been shown to aid fold class assignment. Specifically the combination of vibrational absorption (VA), vibrational circular dichroism (VCD), Raman and Raman optical activity (ROA) in combination with molecular dynamics simulations and density functional theory (DFT) theory calculations has been shown to be able to determine the backbone (secondary structure) of L-alanine, *N*-acetyl L-alanine *N*′-methylamide, L-alanyl L-alanine and Leu-enkephalin [1–3,22,23,25–30] and the side chain conformation of L-histidine [31]. Preliminary studies documenting the use of neural networks to predict the structure of peptides based on a combination of experimental and DFT simulated VA, VCD, Raman spectra have appeared [32,33]. A very feasible extension of this work is to use the characteristic VA, VCD, Raman and ROA spectra of proteins of known fold class and combine with the above aforementioned work on sequences with known structures, to predict the fold class of an unknown protein not only from the sequence, but also from the measured VA, VCD, Raman and ROA spectra [34,35].

To date a complete understanding of the VA, VCD, Raman and ROA spectra is not known to the extent that the combination can be used to determine the complete secondary structure of all residues and how these secondary structural elements fold up to form the tertiary structure. But many believe that the information is present in these spectra, it is just a matter of developing a transparent method which is capable of "processing" the spectra into backbone angles, then side chain angles and finally the packing/interface interactions which are responsible for tertiary structure formation and stability. Our preliminary work above, shows that this work is well worth pursuing, and is being pursued by us and other groups (Keiderling group in Chicago, for example). An accompanying article in this special issue by Ramnarayan, Bohr and Jalkanen discusses this in more detail [36].

Experimental approaches to assigning the characteristic vibrational bands in the IR/VA spectra due to amino acid residues [37] and amides groups in peptides [38] have also been developed. Here one measures the spectra of amino acids and peptides and fits the spectra to determine the vibrational frequencies and dipole strengths (molar extinction coefficients). Subsequently these characteristic bands have been used to estimate the secondary structure content in proteins [39]. In addition to the zwitterionic species, the measurements have been made at various pH values, which allows one to measure the spectra of the cationic and anionic species also. These spectra are important if one is to subtract out the spectra of the side chains of proteins to determine the spectra due to the backbone, which determines the secondary structure

of the protein. The amide I region of the spectra has been used to determine the percentage of various secondary structural elements in the protein [40]. Since the amide I mode is largely composed of the C=O stretch frequency, which is very sensitive to hydrogen bonding, this has been very useful to date. But to do so, requires one to deconvolute the amide I region into its characteristic parts. Here one has measured the spectra of proteins with known secondary structure and then determined the principle component (characteristic) spectra. In addition to these experimental techniques, computational attempts have also been made to determine the molecular species which contribute to the infrared spectra of acids in aqueous solution [41]. A review article on hydrogen bonding has recently appeared which documents the breadth of the different experimental and theoretical techniques used to try to understand hydrogen bonding, in addition to the techniques which we advocate here in this work [42]. Finally the work by Gorelsky and Solomon in this special issue gives an example of the changes in the electronic charge distribution due to oxidation [43,44]. In the case of L-alanine, the zwitterionic species is stabilized by the neighboring solvent molecules, without which the negative electronic charge on the COO^- group is not stable with respect to proton transfer from the positively charged NH_3^+ group. Hence it would be nice to see an extended charge decomposition analysis of the two species of L-alanine within the various models used here, that is, explicit solvent models, continuum solvent models and finally the hybrid where one combines the two models.

In addition to the VA, VCD, Raman and ROA spectra we foresee the use of the electronic absorption (EA) and electronic circular dichroism (ECD) spectra to be of use [40,45,46]. Recently the feasibility of the calculation of all of the aforementioned spectra has been shown, but mostly in the gas phase, using continuum solvent models, using explicit water molecules and finally combining these approaches [1,3,29]. If one can fully understand the changes which occur in the vibrational, electronic and NMR spectra of biomolecules under a variety of experimental conditions by modeling studies, then one can extract information from the spectra of proteins, small flexible ligands (drug molecules) and the changes which occur in both when combined [47–49]. To be able to model these changes one is required to treat not only the few strongly H-bonded water molecules, but also the complete solvent shell around the molecules, and how this shell is changed as the molecule moves from the polar to nonpolar medium. Here we have initially treated the zwitterion in a droplet model, so the nonpolar medium is the vacuum around the droplet. In a future work we will look at a two phase system, for example, a hydrocarbon and water, but here we look at the simplest two phase model. The molecular dynamics simulations were used to generate the snapshots which were used for further analysis. This work contrasts the work done on using soft X-ray spectroscopy to understand the properties of water by studying ice [50]. In addition, to be able to compare the calculated electrical properties with the experimental values one must take into account the vibrational corrections [51,52]. Hence not only is vibrational analysis important for structure, conformation and functional studies, but it is important to be able to evaluate the theoretical methods being developed to determine the electrical and magnetic properties of materials, which have been shown to be dependent on the vibrational levels and populations. The interpretation and use of the wealth of accumulated VA, VCD, Raman and ROA spectra for biomolecules has to date really been limited by the ability to perform high level ab initio and DFT spectral simulations where the effects of the environment have been properly and adequately taken into account [53–56]. In this work we document a methodology which should be used and which hopefully will open the doors for the use of these combined spectroscopies in many applications in molecular biology, molecular biophysics and physical biochemistry. The limitations which previously hindered the interpretation of the effects of the strongly interacting environment have to a large extent been overcome.

2 Methodology

2.1 Treatment of solvent

The treatment of the aqueous environment surrounding and responsible for stabilizing the zwitterionic species of L-alanine (LAZ) has been very interesting. Initially one can treat the environment by using only a continuum model, but this has been shown not to be adequate for strongly interacting H-bonding solvents like water [1,3]. This has complicated the problem because one then has to choose the number of water molecules to include and their positions. Previous workers have used either chemical intuition or classical MD simulations to position the water molecules [1–3,27,57]. Here we have extracted them from density functional Born–Oppenheimer molecular dynamics simulations (DFT BOMD). In addition, there have specifically parametrized molecular mechanics force fields for water, e.g. the TIP5P [58], and also specifically parametrized hybrid exchange correlations functionals to reproduce the electronic properties for water [59].

The positions of the water molecules were extracted from the lowest energy structures from the DFT BOMD simulation for the L-alanine zwitterion [60]. The structure from molecular dynamics simulations was then used for preparation of the initial structure of the L-alanine zwitterion with only a first hydration shell by removing water molecules which are farther than 3.5 from any atom of the alanine molecule. All in all,

only 20 water molecules were required to fully encapsulate (surround) the amino acid. The number of water molecules is sufficient to complete the first hydration shell completely surrounding the L-alanine zwitterion. The network of 20 water molecules have explicit hydrogen bonding interactions with ammonium and carboxylate sites of the L-alanine.

This is the way to treat the first solvation shell of solvent molecules explicitly, rather than to use one of the many continuum solvent model treatments. Additionally we have embedded the L-alanine + 20 water molecules clusters within various continuum models, the Onsager [61], the polarized continuum model (PCM) [62] and the *Co*nductor *S*creening *Mo*del (COSMO) [63–67]. These models can be used to model the effects due to the so-called bulk water molecules. Recent X-ray and neutron diffraction studies have shown that there are two kinds of solvent molecules, those near the surface of the biomolecules which have reduced mobility and density, and those in the bulk solvent [4,68]. A few recent reviews on implicit solvent models have appeared, which give more detail that is possible in our work on vibrational spectroscopy [69–71]. In addition, one can utilize the so-called QM/MM methods [72]. Here one can treat the solute molecule, here LA or NALANMA, by quantum mechanical methods and the aqueous environment by classical molecular mechanic methods. Finally one can try to determine the positions and properties of the aqueous environment surrounding amino acids by combined empirical potential structure refinement (EPSR) fits to diffraction data [73]. This method is in many ways complementary to the methods which we have used.

2.2 Hessian and vibrational frequencies

To determine whether a structure is a local minimum, one normally calculates the second derivatives with respect to nuclear displacements, the so-called force constant matrix or Hessian. By diagonalizing the mass weighted Hessian, one gets the vibrational frequencies within the mechanical harmonic approximation. For a local minimum all of the frequencies should be positive. For a transition state one of the frequencies should be negative. Initially the Hessians within DFT were calculated by finite difference methods [74] and subsequently analytical Hessians have been implemented which has increased the efficiency [75]. In addition, the analytical gradients for the derivative of the energy of an excited state with DFT has also been reported, allowing for the optimization of the geometry of the electronic excited state [76]. Initially one used Hartree-Fock (HF) Hessians to interpret the vibrational spectra of simple organic molecules, but subsequent work showed that one could improve the agreement between the calculated and experimental spectra by scaling the HF Hessians [77–80]. Here one used symmetric molecules where the experimental spectra were assigned so that one could develop scale factors which could then be transferred to other molecules. This methodology has also been used in determining the so-called molecular mechanics force fields [81]. When one has gone to the MP2 and DFT with the hybrid and meta hybrid XC functionals levels of theory, the accuracy has been sufficient such that many groups no longer feel the need to scale the MP2 or DFT force fields. This is the approach we have taken in this work. The agreement could of course be improved by scaling the DFT force fields, but then one would lose the ability to evaluate the errors remaining in the differences between the calculated harmonic frequencies and intensities and the anharmonic frequencies and intensities one gets from the experimental spectra.

2.3 Vibrational absorption

To simulate the vibrational absorption (VA) spectra of a molecule, one first requires an optimized geometry. Hence the LA + 20 water molecule cluster was optimized at the B3LYP/6-31G* optimized level of theory. Additionally the LA + 20 water molecule + (Onsager or PCM or COSMO continuum model) clusters were also optimized at the B3LYP/6-31G* level of theory. At the optimized geometries, the Hessians and atomic polar tensors (APTs) were calculated. By diagonalizing the mass weighted Hessian, one obtains the harmonic frequencies and atomic displacements, the so-called mechanical harmonic approximation. If one also calculates the APTs, the derivatives of the electric dipole moment with respect to nuclear coordinate displacements, one can calculate the VA intensities within the so-called electric harmonic approximation. Here the selection rule gives us that the dipole strengths for the harmonic vibrational transitions are given by [82,83]:

$$\epsilon(\bar{\nu}) = \frac{8\pi^3 N_A}{3,000hc(2.303)} \sum_i \bar{\nu} D_i f_i(\bar{\nu}_i, \bar{\nu}) \tag{1}$$

where ϵ is the molar extinction coefficient, D_i is the dipole strength of the ith transition of wavenumbers $\bar{\nu}_i$ in cm^{-1}, and $f(\bar{\nu}_i, \bar{\nu})$ is a normalised line-shape function and N_A is Avogadro's number.

For a fundamental ($0 \rightarrow 1$) transition involving the ith normal mode within the harmonic approximation

$$D_i = \left(\frac{\hbar}{2\omega_i}\right) \sum_\beta \left\{ \sum_{\lambda\alpha} S_{\lambda\alpha,i} \mu_\beta^{\lambda\alpha} \right\} \left\{ \sum_{\lambda'\alpha'} S_{\lambda'\alpha',i} \mu_\beta^{\lambda'\alpha'} \right\} \tag{2}$$

where $\hbar\omega_i$ is the energy of the ith normal mode, the $S_{\lambda\alpha,i}$ matrix interrelates normal coordinates Q_i to Cartesian displacement coordinates $X_{\lambda\alpha}$, where λ specifies a nucleus and $\alpha = x$, y or z:

$$X_{\lambda\alpha} = \sum_i S_{\lambda\alpha,i} Q_i \tag{3}$$

$\mu_\beta^{\lambda\alpha}$ (α, $\beta = x,y,z$) are the APT of nucleus λ. $\mu_\beta^{\lambda\alpha}$ are defined by

$$\mu_\beta^{\lambda\alpha} = \left\{ \frac{\partial}{\partial X_{\lambda\alpha}} < \psi_G(\mathbf{R}) | (\mu_{el})_\beta | \psi_G(\mathbf{R}) > \right\}_{\mathbf{R}_o} \tag{4}$$

$$\mu_\beta^{\lambda\alpha} = 2 \left\langle \left(\frac{\partial \psi_G(\mathbf{R})}{\partial X_{\lambda\alpha}} \right)_{\mathbf{R}_o} \mid \left(\mu_{el}^e\right)_\beta \mid \psi_G(\mathbf{R}_o) \right\rangle + Z_\lambda e \delta_{\alpha\beta} \tag{5}$$

where $\psi_G(\mathbf{R})$ is the electronic wavefunction of the ground state G, $\mathbf{R}$ specifies nuclear coordinates, $\mathbf{R}_o$ specifies the equilibrium geometry, $\boldsymbol{\mu}_{el}$ is the electric dipole moment operator, $\bar{\mu}_{el}^e = -e \sum_i \bar{r}_i$ is the electronic contribution to $\bar{\mu}_{el}$ and $Z_\lambda e$ is the charge on nucleus λ.

The problem with the expression for the APT presented is that it involves the wavefunction, and wavefunction derivatives, (usually calculated with Coupled Perturbed Hartree-Fock theory) [84–88]. These equations extend the Roothan-Hall equations for perturbations [89–91]. These expressions have been implemented in CADPAC to calculate the APT at the SCF and MP2 levels. The advantages of DFT are numerous but the main one for us is to extend rigorous methodology to the calculation of properties of large biological molecules. DFT seems to provide a way to do that. But the expressions must be reformulated as expressions amenable for DFT, that is, as energy derivatives. The APT tensors have also been implemented at the DFT level in Gaussian 03, CADPAC and Dalton [92] using Gaussian orbitals and in the Amsterdam Density Functional (ADF) code using Slater orbitals [93–95]. Since in DFT one must do many numerical integrations, the advantages of using Gaussian orbitals is lost to some extent. Investigations of the performance of local, gradient-corrected and hybrid density functional models in predicting infrared/VA intensities have shown that the hybrid functionals are very accurate when the solvent effects are not important [96,97]. To date there has not been a systematic investigation of the prediction of infrared/VA intensities in strongly hydrogen bonded solvents. The problem here has been that the solvent absorbs significantly and also that there are strong interactions between the solute and solvent. Hence the conclusions based on previous studies where the solvent effects were negligible are not necessarily applicable to the strongly hydrogen bonding systems. Here the use of explicit solvent molecules, continuum solvent models, hybrid models which combine the two aforementioned approaches or a molecular dynamics simulation approach are all methods which have been used in limited numbers of cases, but no systematic study has been undertaken. This has to some extent been limited by the complexity and no general consensus on which properties need to be evaluated. Here we would suggest/recommend that the vibrational frequencies and VA intensities be mandatory, as the amide I region of the spectra of proteins has been used to date without a complete understanding of the various contributions to the linewidths and intensities due to the specific secondary structural elements. This work documents part of that complexity which we have investigated in this work.

For periodic systems the concept of atomic polar tensors of the molecular system embedded within a solid is a more complex concept. Here one introduces the Born effective charge, Z^*, that describes the polarization created by atomic displacements [98].

$$Z^*_{\kappa,\alpha\beta} = \Omega_o \left. \frac{\partial P_\beta}{\partial \tau_{\kappa\alpha}} \right|_{\varepsilon=0} \tag{6}$$

2.4 Vibrational circular dichroism

If one wishes to simulate the vibrational circular dichroism (VCD) spectra, in addition, to the VA spectra, one is required to calculate the atomic axial tensors (AATs) [99–105]. The AAT are the derivatives of the magnetic dipole moment with respect to the nuclear velocities [106,107]. Hence within the Born-Oppenheimer approximation [108], the electronic contribution to the AAT are zero [109]. Stephens and Buckingham have shown that the electronic contributions can be calculated by a variety of different formulations. Additionally, the problem of the gauge dependence of the tensors has been treated in a variety of ways, the so-called common origin gauge with very large basis sets, and the distributed origin gauge [101,110]. Here one has used the traditional basis sets, which are not dependent on the perturbation, be it an electric or a magnetic field. Another way to treat the gauge problem is to add magnetic field dependent orbitals, the so-called London atomic orbitals. Finally one can use molecular orbitals which depend on the magnetic field, the so-called LORG method of Bouman and Hansen [111]. All of the aforementioned methods have been shown to give very similar, equivalent and accurate values for the AATs if one uses very large basis sets, what is different among the various methods is how fast the AATs converge to the limiting values as a function of basis set. If one is limited to relatively small basis sets, as we are here, the use of gauge invariant atomic orbitals appears to be the method of choice [112–114].

The vibrational circular dichroism spectra is related to the molecular rotational strengths via,

$$\Delta\epsilon(\bar{\nu}) = \frac{32\pi^3 N}{3,000hc(2.303)} \sum_i \bar{\nu} R_i f_i(\bar{\nu}_i, \bar{\nu}) \tag{7}$$

where $\Delta\epsilon = \epsilon_L - \epsilon_R$ is differential extinction coefficient and R_i is the rotational strength of the ith transition of wavenumbers $\bar{\nu}_i$ in cm^{-1}, and $f(\bar{\nu}_i, \bar{\nu})$ is a normalized line-shape function and N_A is Avogadro's number.

$$R_i = \hbar^2 Im \sum_\beta \left\{ \sum_{\lambda\alpha} S_{\lambda\alpha,i} \mu_\beta^{\lambda\alpha} \right\} \left\{ \sum_{\lambda'\alpha'} S_{\lambda'\alpha',i} m_\beta^{\lambda'\alpha'} \right\} \tag{8}$$

where $\hbar\omega_i$ is the energy of the ith normal mode, the $S_{\lambda\alpha,i}$ matrix interrelates normal coordinates Q_i to Cartesian displacement coordinates $X_{\lambda\alpha}$, where λ specifies a nucleus and $\alpha = x, y$ or z: $X_{\lambda\alpha}$ is as previously defined. $\mu_\beta^{\lambda\alpha}$ and $m_\beta^{\lambda\alpha}$ (α, β = x,y,z) are the APT and AAT of nucleus λ.

$\mu_\beta^{\lambda\alpha}$ is as previously defined and $m_\beta^{\lambda\alpha}$ is given by

$$m_\beta^{\lambda\alpha} = I_\beta^{\lambda\alpha} + \frac{i}{4\hbar c}\sum_\gamma \epsilon_{\alpha\beta\gamma} R^o_{\lambda\gamma}(Z_\lambda e) \tag{9}$$

$$I_\beta^{\lambda\alpha} = \left\langle \left(\frac{\partial\psi_G(\mathbf{R})}{\partial X_{\lambda\alpha}}\right)_{\mathbf{R}_e} \middle| \left(\frac{\partial\psi_G(\mathbf{R}_e, B_\beta)}{\partial B_\beta}\right)_{B_\beta=0} \right\rangle \tag{10}$$

where $\psi_G(\mathbf{R}_o, B_\beta)$ is the ground state electronic wavefunction in the equilibrium structure $\mathbf{R}_e$ in the presence of the perturbation $-(\mu^e_{\mathrm{mag}})_\beta B_\beta$, where $\boldsymbol{\mu}^e_{\mathrm{mag}}$ is the electronic contribution to the magnetic dipole moment operator. $m_\beta^{\lambda\alpha}$ is origin dependent. Its origin dependence is given by

$$(m_\beta^{\lambda\alpha})^0 = (m_\beta^{\lambda\alpha})^{0'} + \frac{i}{4\hbar c}\sum_{\gamma\delta}\epsilon_{\beta\gamma\delta} Y^\lambda_\gamma \mu^{\lambda\delta}_\alpha \tag{11}$$

where $\mathbf{Y}^\lambda$ is the vector from O to O′ for the tensor of nucleus λ. Equation (10) permits alternative gauges in the calculation of the set of $(m_\beta^{\lambda\alpha})^0$ tensors. If $\mathbf{Y}^\lambda = 0$, and hence O = O′, for all λ the gauge is termed the Common Origin (CO) gauge. If $\mathbf{Y}^\lambda = \mathbf{R}^o_\lambda$, so that in the calculation of $(m_\beta^{\lambda\alpha})^0$ O′ is placed at the equilibrium position of nucleus λ, the gauge is termed the DO gauge [101,102].

Density functional theory atomic axial tensors have also been implemented in Gaussian 94 [115]. We have utilized Gaussian 03 to calculate the B3LYP/6-31G* AAT in this work. Note that the AAT have been implemented within both the PCM and COSMO continuum models within Gaussian 03, but not yet with the simplest Onsager continuum model. The VCD simulations for the Onsager calculations utilize the AAT calculated without a continuum solvent treatment. The AAT have also recently been implemented in the ADF code which utilizes Slater type orbitals rather than the Gaussian type orbitals used in Gaussian, CADPAC and Dalton [95].

2.5 Raman scattering

If one wishes to simulate the Raman scattering intensities, one is required to calculate the electric dipole-electric dipole polarizability derivatives. Here one can use either the static values, as has been done in most works to date, or one can take into account the frequency response. In most conventional Raman scattering experiments one uses either a 488 or 1,064 nm source, the later for molecules for which fluorescence is a problem.

The Raman intensity is proportional to the Raman scattering activity, which is given for the jth normal mode Q_j by:

$$I_j^{\mathrm{Ram}} = g_j(45\bar{\alpha}_j^2 + 7\bar{\beta}_j^2), \tag{12}$$

where g_j is the degeneracy of the jth transition, and the electric dipole-electric dipole polarizability tensor derivative invariants $\bar{\alpha}_j^2$ and $\bar{\beta}_j^2$ are given by:

$$\bar{\alpha}_j^2 = \frac{1}{9}\left(S_{\lambda\alpha,j}\alpha^{\lambda\alpha}_{xx} + S_{\lambda\alpha,j}\alpha^{\lambda\alpha}_{yy} + S_{\lambda\alpha,j}\alpha^{\lambda\alpha}_{zz}\right)^2 \tag{13}$$

and

$$\begin{aligned}\bar{\beta}_j^2 = \frac{1}{9}\Big\{&\left(S_{\lambda\alpha,j}\alpha^{\lambda\alpha}_{xx} - S_{\lambda\alpha,j}\alpha^{\lambda\alpha}_{yy}\right)^2 + \Big(S_{\lambda\alpha,j}\alpha^{\lambda\alpha}_{xx} \\ &- S_{\lambda\alpha,j}\alpha^{\lambda\alpha}_{zz}\Big)^2 + \left(S_{\lambda\alpha,j}\alpha^{\lambda\alpha}_{yy} - S_{\lambda\alpha,j}\alpha^{\lambda\alpha}_{zz}\right)^2 \\ &+ 6\left[\left(S_{\lambda\alpha,j}\alpha^{\lambda\alpha}_{xy}\right)^2 + \left(S_{\lambda\alpha,j}\alpha^{\lambda\alpha}_{yz}\right)^2 + \left(S_{\lambda\alpha,j}\alpha^{\lambda\alpha}_{xz}\right)^2\right]\Big\},\end{aligned} \tag{14}$$

respectively. The $S_{\lambda\alpha,j}$ matrix relates the normal coordinates Q_j to the Cartesian displacement coordinates $X_{\lambda\alpha}$, where λ specifies a nucleus and α = x, y or z [116], as previously defined.

The normal frequencies are the eigenvalues Λ of the mass weighted Hessian matrix (the Hessian matrix, H, being the matrix of the second derivatives of the energy with respect to nuclear displacements, evaluated at the equilibrium geometry):

$$H_{\lambda\alpha,\lambda'\alpha'} = \left(\frac{\partial^2 E(\mathbf{R})}{\partial X_{\lambda\alpha}\partial X_{\lambda'\alpha'}}\right)_{\mathbf{R}=\mathbf{R}_o} \tag{15}$$

and

$$C^{-1}HC = \Lambda. \tag{16}$$

C is the eigenvector matrix, which defines the transformation matrix S which is given by:

$$S = M^{-1/2}C, \tag{17}$$

where M is the mass matrix.

Therefore, through the matrix S (obtained by diagonalizing the Hessian matrix) and the electric dipole-electric dipole polarizability derivatives (EDEDPD), $\alpha^{\lambda\alpha}_{\beta\gamma}$, one can obtain the Raman scattering activity $\mathrm{I}_j^{\mathrm{Ram}}$ of any normal mode Q_j. The first efficient method for determining the EDEDPD was implemented utilizing finite field perturbation theory by Komornicki 1979 [117]. Subsequently the analytical EDEDPD were derived and implemented in CADPAC [118, 119] and Gaussian [120] at the Hartree-Fock level of theory, and subsequencly at the DFT level. The EDEDPD have also been implemented at the DFT level and used to simulate the Raman spectra without any solvent treatment [97,121–125] and subsequently by treating the solvent with explicit solvent molecules, with continuum solvent models, and finally using hybrid models which combine the two [31,46,126]. In contrast to solvent subtraction which is common in infrared/VA

spectroscopy, this is not always done with Raman measurements. Investigations of the performance of local, gradient-corrected and hybrid density functional models in predicting Raman intensities have shown that the hybrid functionals are very accurate when the solvent effects are not important [96,97].

Hence the question of whether and how to perform a solvent subtraction for Raman measurements is a question which we will address in this work.

2.6 Raman optical activity

Finally if one wishes to simulate the Raman optical activity (ROA) intensities, one is required to calculate the electric dipole-magnetic dipole polarizability derivatives (EDMDPD) and the electric dipole-electric quadrupole polarizability derivatives (EDEQPD) [107,127–130]. The calculation of the EDMDP, G′, have been implemented in CADPAC [131]. The EDMDP can be evaluated as the second derivative of the energy with respect to a static electric field and a time varying magnetic field. Hence the EDMDPD is a third derivative, the third derivative being with respect to the nuclear displacement.

$$G'^{\lambda\alpha}_{\beta\gamma} = \left(\frac{\partial^3 W_G(\mathbf{R}, F_\beta, \dot{B}_\gamma)}{\partial X_{\lambda\alpha}\partial F_\beta \partial \dot{B}_\gamma}\right)_{\mathbf{R}=\mathbf{R}_o, F_\beta=0, \dot{B}_\gamma=0} = \left(\frac{\partial G'_{\beta\gamma}(\mathbf{R})}{\partial X_{\lambda\alpha}}\right)_{\mathbf{R}=\mathbf{R}_o} \tag{18}$$

The electric dipole-electric dipole, electric dipole-magnetic dipole and electric dipole-electric quadrupole polarizability tensors can also be calculated at the frequency of the incident light using SCF linear response theory. For the EDMDPD calculations London atomic orbitals have been employed, and hence the results are gauge invariant [132]. In this work, the electric dipole-magnetic dipole orbitals are gauge independent when using a finite basis set due to the use of gauge invariant atomic orbitals as implemented in Gaussian 03. Previously we used conventional basis sets which were not gauge invariant, similar to the work of Polavarapu et al. [23,133–135] and our previous work on NALANMA [3], where that level of theory had been show to give predicted ROA spectra in good agreement with the experimentally observed spectra. We are thus confident that the new level of theory can be used to answer the structural questions posed here, realizing that the agreement in absolute intensities could be improved by using much larger basis sets, as we shall do for the NALANMA4WC, but not the LA20WC.

The EDEQP, A, can be evaluated as the second derivative of the energy with respect to a static electric field and a static electric field gradient. Hence the EDEQPD is a third derivative, the third derivative being with respect to the nuclear displacement.

$$A^{\lambda\alpha}_{\beta,\gamma\delta} = \left(\frac{\partial^3 W_G(\mathbf{R}, F_\beta, F'_{\gamma\delta})}{\partial X_{\lambda\alpha}\partial F_\beta \partial F'_{\gamma\delta}}\right)_{\mathbf{R}=\mathbf{R}_o, F_\beta=0, F'_{\gamma\delta}=0} = \left(\frac{\partial A_{\beta,\gamma\delta}(\mathbf{R})}{\partial X_{\lambda\alpha}}\right)_{\mathbf{R}=\mathbf{R}_o} \tag{19}$$

The Cartesian polarizability derivatives are required to calculate the ROA spectra. The quantities required have been derived by Barron and Buckingham [127,129,136–138]. The quantities are calculated by combining the various polarizability derivatives with the normal mode vectors in the following equations.

$\bar{\alpha}_j \bar{G}'_j$ is given by:

$$\bar{\alpha}_j \bar{G}'_j = \frac{1}{9}\left(S_{\lambda\alpha,j}\alpha^{\lambda\alpha}_{xx} + S_{\lambda\alpha,j}\alpha^{\lambda\alpha}_{yy} + S_{\lambda\alpha,j}\alpha^{\lambda\alpha}_{zz}\right)\left(S_{\lambda\alpha,j}G'^{\lambda\alpha}_{xx} + S_{\lambda\alpha,j}G'^{\lambda\alpha}_{yy} + S_{\lambda\alpha,j}G'^{\lambda\alpha}_{zz}\right). \tag{20}$$

γ_j^2 is given by:

$$\begin{aligned}\gamma_j^2 = \frac{1}{2}\Big\{&(S_{\lambda\alpha,j}\alpha^{\lambda\alpha}_{xx} - S_{\lambda\alpha,j}\alpha^{\lambda\alpha}_{yy})(S_{\lambda\alpha,j}G'^{\lambda\alpha}_{xx} - S_{\lambda\alpha,j}G'^{\lambda\alpha}_{yy})\\ &+(S_{\lambda\alpha,j}\alpha^{\lambda\alpha}_{xx} - S_{\lambda\alpha,j}\alpha^{\lambda\alpha}_{zz})(S_{\lambda\alpha,j}G'^{\lambda\alpha}_{xx} - S_{\lambda\alpha,j}G'^{\lambda\alpha}_{zz})\\ &+(S_{\lambda\alpha,j}\alpha^{\lambda\alpha}_{yy} - S_{\lambda\alpha,j}\alpha^{\lambda\alpha}_{zz})(S_{\lambda\alpha,j}G'^{\lambda\alpha}_{yy} - S_{\lambda\alpha,j}G'^{\lambda\alpha}_{zz})\\ &+3\Big[(S_{\lambda\alpha,j}\alpha^{\lambda\alpha}_{xy})\,(S_{\lambda\alpha,j}G'^{\lambda\alpha}_{xy} + S_{\lambda\alpha,j}G'^{\lambda\alpha}_{yx})\\ &+(S_{\lambda\alpha,j}\alpha^{\lambda\alpha}_{yz})(S_{\lambda\alpha,j}G'^{\lambda\alpha}_{yz} + S_{\lambda\alpha,j}G'^{\lambda\alpha}_{zy})\\ &+(S_{\lambda\alpha,j}\alpha^{\lambda\alpha}_{xz})(S_{\lambda\alpha,j}G'^{\lambda\alpha}_{xz} + S_{\lambda\alpha,j}G'^{\lambda\alpha}_{zx})\Big]\Big\},\end{aligned} \tag{21}$$

and δ_j^2 is given by:

$$\begin{aligned}\delta_j^2 = \frac{\omega}{2}\Big\{&(S_{\lambda\alpha,j}\alpha^{\lambda\alpha}_{yy} - S_{\lambda\alpha,j}\alpha^{\lambda\alpha}_{xx})S_{\lambda\alpha,j}A^{\lambda\alpha}_{z,xy}\\ &+(S_{\lambda\alpha,j}\alpha^{\lambda\alpha}_{xx} - S_{\lambda\alpha,j}\alpha^{\lambda\alpha}_{zz})S_{\lambda\alpha,j}A^{\lambda\alpha}_{y,zx}\\ &+(S_{\lambda\alpha,j}\alpha^{\lambda\alpha}_{zz} - S_{\lambda\alpha,j}\alpha^{\lambda\alpha}_{yy})S_{\lambda\alpha,j}A^{\lambda\alpha}_{x,yz}\\ &+S_{\lambda\alpha,j}\alpha^{\lambda\alpha}_{xy}(S_{\lambda\alpha,j}A^{\lambda\alpha}_{y,yz} - S_{\lambda\alpha,j}A^{\lambda\alpha}_{z,yy}\\ &+S_{\lambda\alpha,j}A^{\lambda\alpha}_{z,xx} - S_{\lambda\alpha,j}A^{\lambda\alpha}_{x,xz})\\ &+S_{\lambda\alpha,j}\alpha^{\lambda\alpha}_{xz}(S_{\lambda\alpha,j}A^{\lambda\alpha}_{y,zz} - S_{\lambda\alpha,j}A^{\lambda\alpha}_{z,zy}\\ &+S_{\lambda\alpha,j}A^{\lambda\alpha}_{x,xy} - S_{\lambda\alpha,j}A^{\lambda\alpha}_{y,xx})\\ &+S_{\lambda\alpha,j}\alpha^{\lambda\alpha}_{yz}(S_{\lambda\alpha,j}A^{\lambda\alpha}_{z,zx} - S_{\lambda\alpha,j}A^{\lambda\alpha}_{x,zz}\\ &+S_{\lambda\alpha,j}A^{\lambda\alpha}_{x,yy} - S_{\lambda\alpha,j}A^{\lambda\alpha}_{y,yx})\Big\}.\end{aligned} \tag{22}$$

The equations relating these tensor derivatives to the ROA spectra are given by Barron 1982 [136], 2004 [139], Hecht et al. 1989 [140] and Barron et al. 1994 [141]. These references provide a good introduction to the theory and application of ROA spectroscopy. Here we shall give the relevant

equations for completeness. We follow very closely the notation of Barron from his Faraday Discussions review article [141].

The commonly reported quantity from ROA measurements is the dimensionless circular intensity differential (CID) defined as

$$\Delta_\alpha = \left(\frac{I_\alpha^R - I_\alpha^L}{I_\alpha^R + I_\alpha^L}\right), \tag{23}$$

where I_α^R and I_α^L are the scattered intensities with linear α-polarization in right- and left-circularly polarized incident light. In terms of the quantities, EDEDPD, EDMDPD and EDEQPD, the CIDs for forward, backward, and polarized and depolarized right-angle scattering from an isotropic sample for incident laser light are [141]:

$$\Delta(\text{forward}) = \left(\frac{8[45\alpha G' + \beta(G')^2 - \beta(A)^2]}{2c[45\alpha^2 + 7\beta(\alpha)^2]}\right) \tag{24}$$

$$\Delta(\text{backward})_{\text{ICP}} = \left(\frac{48[\beta(G')^2 + (1/3)\beta(A)^2]}{2c[45\alpha^2 + 7\beta(\alpha)^2]}\right) \tag{25}$$

$$\Delta(90^\circ, \text{polarized}) = \left(\frac{2[45\alpha G' + 7\beta(G')^2 + \beta(A)^2]}{c[45\alpha^2 + 7\beta(\alpha)^2]}\right) \tag{26}$$

$$\Delta(90^\circ, \text{depolarized}) = \left(\frac{12[\beta(G')^2 - (1/3)\beta(A)^2]}{6c\beta(\alpha)^2}\right) \tag{27}$$

$$\Delta(\text{backward})_{\text{DCP}_\text{I}} = \left(\frac{48[\beta(G')^2 + (1/3)\beta(A)^2]}{2c[6\beta(\alpha)^2]}\right), \tag{28}$$

where c is the speed of light and the isotropic invariants are defined as

$$\alpha = (1/3)\alpha_{\alpha\alpha} \tag{29}$$

and

$$G' = (1/3)G'_{\alpha\alpha}, \tag{30}$$

and the anisotropic invariants as

$$\beta(\alpha)^2 = (1/2)(3\alpha_{\alpha\beta}\alpha_{\alpha\beta} - \alpha_{\alpha\alpha}\alpha_{\beta\beta}) \tag{31}$$

$$\beta(G')^2 = (1/2)(3\alpha_{\alpha\beta}G'_{\alpha\beta} - \alpha_{\alpha\alpha}G'_{\beta\beta}) \tag{32}$$

$$\beta(G')^2 = (1/2)(3\alpha_{\alpha\beta}G'_{\alpha\beta} - \alpha_{\alpha\alpha}G'_{\beta\beta}) \tag{33}$$

$$\beta(A)^2 = (1/2)\omega\alpha_{\alpha\beta}\epsilon_{\alpha\gamma\delta}A_{\gamma\delta\beta}. \tag{34}$$

Using these expressions we can calculate the ROA spectra within the harmonic approximation for the vibrational frequencies and with the static field limit for the EDEDPD, EDMDPD and EDEQPD.

3 Results

3.1 Structures of the L-alanine zwitterion

In Fig. 1 we show the optimized L-alanine + 20 water molecule cluster (LA20WC) optimized structure as determined at the OPBE0/TZ2P + COSMO level of theory as calculated with the Amsterdam Density Functional (ADF) code [93, 95]. Additionally, the LA20WC and the LA20WC embedded within the Onsager, PCM and COSMO continuum models have been calculated at the B3LYP/6-31G* and B3PW91 levels of theory. In Table 1 the geometrical parameter for L-alanine are reported for the eight new models for the B3LYP/6-31G* and B3PW91 hybrid exchange correlation (XC) functionals, as well as some of the previously reported values and the values reported from an experimental crystal structure determination. A comparison of the L-alanine zwitterion stabilized by interactions in the crystal with the LAZ stabilized by water molecules in molecular complexes with varying numbers of waters has also been discussed [6]. The initial model by Barron et al. [134] was at the Hartree-Fock level without any treatment of the aqueous environment, the second model by Yu et al. [142] was again at the Hartree-Fock level but including the Onsager continuum model. The models of Tajkhorshid et al. [1] and Frimand et al. [2] both included explicit water molecules in addition to the Onsager continuum model, but the water molecules included were only those which were directly H-bonded with the ammonium and carboxylate groups. Here the water molecule layer completely encapsulated the L-alanine. Only the geometry of the L-alanine zwitterion is given in Table 1. The complete set of coordinates are available as supplementary material.

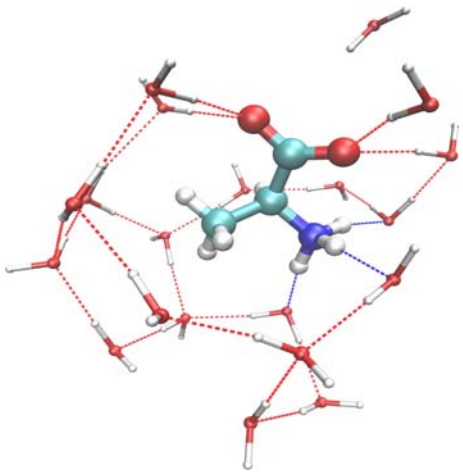

Fig. 1 L-alanine + 20 water molecules at OPBE0/TZ2P + COSMO level of theory

Table 1 L-alanine zwitterion structure table

Coordinate	F′	F‴	Ba	Yu′	Lh	I	II	III	IV	I′	II′	III′	IV′
r(N2–C3)	1.5059	1.4975	1.5120	1.5123	1.495	1.489	1.489	1.491	1.490	1.480	1.482	1.482	1.481
r(C3–C4)	1.5621	1.5526	1.5714	1.5616	1.537	1.535	1.537	1.536	1.540	1.528	1.526	1.534	1.534
r(C4–O5)	1.2812	1.2649	1.2463	1.2329	1.266	1.266	1.247	1.264	1.249	1.250	1.256	1.245	1.247
r(C4–O6)	1.2461	1.2633	1.2061	1.2352	1.249	1.265	1.284	1.267	1.280	1.278	1.275	1.277	1.277
r(C3–C7)	1.5296	1.5322	1.5174	1.5223	1.534	1.532	1.530	1.530	1.532	1.526	1.527	1.526	1.526
r(C3–H8)	1.0945	1.0955	1.0810	1.0824	1.032	1.093	1.094	1.093	1.096	1.094	1.094	1.096	1.096
r(N2–H12)	1.0447	1.0477	1.0056	1.0140	1.050	1.033	1.044	1.036	1.053	1.036	1.036	1.056	1.054
r(N2–H13)	1.0442	1.0540	1.0654	1.0135	1.034	1.077	1.060	1.063	1.056	1.073	1.056	1.057	1.057
r(N2–H1)	1.0462	1.0519	1.0045	1.0112	1.039	1.054	1.047	1.055	1.055	1.056	1.063	1.056	1.057
r(C7–H9)	1.0958	1.0956	1.0863	1.0839	1.096	1.094	1.093	1.094	1.095	1.094	1.094	1.094	1.094
r(C7–H10)	1.0919	1.0947	1.0804	1.0806	1.097	1.091	1.089	1.091	1.091	1.091	1.091	1.091	1.091
r(C7–H11)	1.0948	1.0922	1.0862	1.0861	1.096	1.090	1.094	1.089	1.094	1.090	1.090	1.093	1.093
θ(N2–C3–C4)	112.14	113.52	103.87	109.27	110.00	111.14	110.87	110.67	110.17	110.68	110.63	110.34	110.55
θ(C3–C4–O5)	118.65	119.22	112.11	115.80	118.30	118.30	119.68	118.16	118.84	118.74	118.34	118.44	119.06
θ(C3–C4–O6)	114.46	114.85	115.17	115.34	116.00	115.90	115.21	115.95	115.81	116.00	116.76	116.05	115.68
θ(N2–C3–C7)	109.38	109.07	112.19	109.72	109.80	111.09	109.93	110.84	111.14	110.70	110.59	110.93	111.05
θ(C4–C3–C7)	112.02	111.69	113.55	115.02	111.20	108.57	111.42	108.86	110.70	108.14	108.18	110.12	110.71
θ(N2–C3–H8)	106.23	106.47	107.09	105.21	107.00	106.47	106.05	106.65	106.84	106.97	106.93	107.12	106.84
θ(C4–C3–H8)	115.12	106.48	108.83	107.44	108.34	109.13	108.69	109.34	108.20	110.05	110.20	108.48	107.94
θ(C3–N2–H12)	108.65	113.76	113.40	112.50	108.90	110.46	112.34	110.47	111.79	109.69	109.98	111.64	111.54
θ(C3–N2–H13)	109.71	111.76	97.53	107.96	109.30	107.15	110.57	108.01	108.40	107.29	108.11	108.60	108.38
θ(H12–N2–H13)	107.35	107.21	110.31	107.05	110.25	111.03	111.79	110.07	109.96	110.85	110.21	110.24	110.87
θ(C3–N2–H1)	111.83	105.65	114.57	113.45	111.20	109.81	107.31	110.64	110.08	110.01	109.88	109.88	109.87
θ(H12–N2–H1)	109.09	107.36	108.78	105.76	108.74	106.68	107.63	106.77	107.97	106.40	106.39	108.10	107.78
θ(C3–C7–H9)	110.61	110.53	111.02	111.09	110.10	110.88	111.04	110.88	111.34	110.78	111.03	111.20	111.21
θ(C3–C7–H10)	108.74	110.57	107.92	108.49	110.30	110.02	110.32	109.85	109.66	110.16	110.25	109.79	109.80
θ(H9–C7–H10)	108.68	108.44	107.58	113.40	108.33	108.31	108.40	108.41	108.18	108.69	108.72	108.28	108.29
θ(C3–C7–H11)	110.88	109.24	112.29	111.86	110.10	110.34	110.90	110.57	110.99	110.18	110.21	111.00	110.88
θ(H9–C7–H11)	108.61	108.82	108.92	108.32	110.68	108.63	108.41	108.75	108.53	108.43	108.40	108.44	108.46
τ(N2–C3–C4–O5)	-2.76	-3.54	4.29	8.28	-18.60	-34.60	-16.61	-34.02	-15.36	-29.48	-30.48	-15.51	-14.21
τ(N2–C3–C4–O6)	177.18	176.44	-175.97	-173.83	161.50	150.59	163.92	150.71	165.26	155.37	154.14	165.75	166.29
τ(C4–C3–N2–H12)	60.12	67.56	111.36	93.89	60.49	58.91	72.71	58.53	64.41	58.20	59.43	62.14	64.06
τ(C4–C3–N2–H13)	-56.96	-54.22	-4.66	-24.00	-60.01	-62.15	-52.94	-61.91	-58.95	-62.28	-60.95	-59.62	-58.27
τ(C4–C3–N2–H1)	-179.42	-175.00	-122.93	-146.11	-179.71	176.29	-169.19	176.54	-177.61	174.90	176.22	-177.94	-176.50
τ(H9–C7–C3–H8)	170.62	177.65	177.29	178.29	176.04	-169.39	-174.62	-170.26	-174.76	-171.97	-169.45	-174.49	-175.98
τ(H10–C7–C3–H8)	-70.10	-62.64	-65.05	-58.21	-64.46	-49.59	-54.42	-50.45	-55.03	-51.67	-48.89	-54.68	-56.14
τ(H11–C7–C3–H8)	50.06	57.55	55.08	57.11	53.74	70.21	64.77	69.04	64.26	68.06	70.43	64.69	63.25

r is in Ångstrøm, θ and τ in degrees
F′ B3LYP/6-31G* LA zwitterion + 4H_2O + Onsager from [1]
F‴ B3LYP/6-31G* LA zwitterion + 9H_2O from [2]
Ba RHF/6-31G* zwitterion, from Barron et al. 1991 [134]
Yu′ RHF/6-31G* level LA zwitterion, from [142]
Lh Experimental crystalline LA zwitterion, from [181]
I B3LYP/6-31G* LA zwitterion + 20H_2O
II B3LYP/6-31G* LA zwitterion + 20H_2O + Onsager
III B3LYP/6-31G* LA zwitterion + 20H_2O + PCM
IV B3LYP/6-31G* LA zwitterion + 20H_2O + COSMO
I′ B3PW91/6-31G* LA zwitterion + 20H_2O
II′ B3PW91/6-31G* LA zwitterion + 20H_2O + Onsager
III′ B3PW91/6-31G* LA zwitterion + 20H_2O + PCM
IV′ B3PW91/6-31G* LA zwitterion + 20H_2O + COSMO

3.2 VA spectra for L-alanine

In Fig. 2 we present the simulated VA spectra at the B3LYP/6-31G* level of theory for the LA20WC, LA20WC plus Onsager continuum solvent model, LA20WC plus PCM continuum solvent model and finally the LA20WC plus the COSMO continuum solvent model. As one can see the effects of including the various continuum solvent models for the treatment of the bulk waters are not all the same. The way to determine the optimum continuum solvent model is to compare to the experimental VA spectra. As one can see when one compares the four simulated spectra to the experimental one, there appears to be a systematic shift in the spectra. This can be accounted for by two effects: (i) the harmonic approximation used which is known to overestimate the anharmonic frequencies and (ii) the use of a split valence plus polarization only on carbon, nitrogen and oxygen basis set (6-31G*). We have previously shown that one can do much better by using the aug-cc-pVDZ and aug-cc-pVTZ basis sets for VA, VCD, Raman and ROA spectral simulations for phenyloxirane [97]. In addition, in this special issue the Keiderling group has utilized the 6-311++G** basis set with the B3LYP and B3PW91 hybrid exchange correlation functional to simulate the VA spectra for some idealized turn structures [143]. Here they have not attempted to do a systematic search to determine the lowest energy conformer of the molecules studied, but rather have used the molecule in its ideal turn structures to try to identify the characteristic features in the VA (and VCD) spectrum which can be used in their works on proteins. The question of the interactions which stabilize these structures in real proteins and makes these structures the global minimum were not addressed and thought not to be important in the VA and VCD spectra. But the effects of some of the environment were taken into account by adding some explicit water molecules. In many cases one compares to only the gas phase experiments and one does not then have to deal with the effects of the environment, since there is none [144]. Clearly these methods need to be extended to deal with the effects due to strongly interacting environments, for example, hydrogen bonding solvents like water. But then two problems appear, one how to initially treat the hydrogen bonded molecules in not only the structure determination, but also the spectral simulations. In many cases one runs a solvent spectra and then presents the solvent subtracted spectra. For the simulations to be able to reproduce, interpret and understand these spectra, and the conformational and solvent fluctuations and changes which contribute to them, then the simulations must be run long enough to deal with the sampling problems. In addition, there are inherent assumptions made by the experimentalists which can be checked, verified and confirmed, or not verified and not confirmed. Hence there is clearly more work to do beyond the approach which we have taken in this work, and we look forward to presenting our contributions to this new approach in a future publication. But here it is important to point out some of the inherent pitfalls and challenges which should be considered and taken into account so that other groups can benefit from the work to date.

3.3 VCD spectra for L-alanine

In Figs. 3 we present the simulated VCD spectra at the B3LYP/6-31G* level of theory for the LA20WC, LA20WC plus Onsager continuum solvent model, LA20WC plus PCM continuum solvent model and finally the LA20WC plus the COSMO continuum solvent model. Here we also see that VCD spectra is also affected by the various ways to treat the

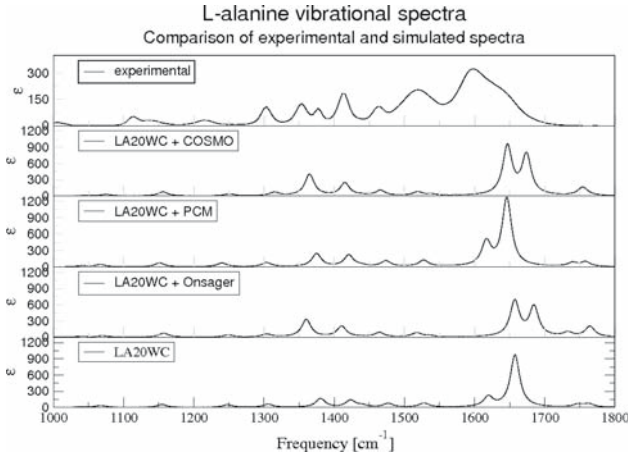

Fig. 2 Comparison of VA spectra for B3LYP/6-31G* LA20WC, LA20WC + Onsager, LA20WC + PCM and LA20WC + COSMO and experiment

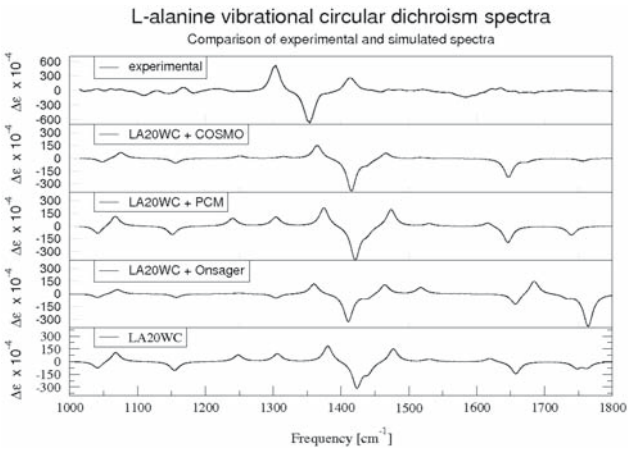

Fig. 3 Comparison of VCD spectra for B3LYP/6-31G* LA20WC, LA20WC + Onsager, LA20WC + PCM and LA20WC + COSMO and experiment

bulk water molecules. We shall once again use the comparison to the experimental VCD spectra as our method to determine which continuum solvent model is optimum for this purpose. As one can see in Fig. 3, the agreement between the four theoretical VCD spectra with the experimental spectra is quite good, taking into account the aforementioned differences due to the harmonic approximation and the use of the 6-31G* basis set. This is to be expected since the number of water molecules has been increased to now fully encapsulate the LAZ. The effects due to the continuum solvent treatments are now to treat the effects due to the second solvation shell water molecules and the bulk. The initial question of fully encapsulating the LAZ has hence been addressed in this work.

Previously experimental work on the VCD of the LAZ has also appeared both with dispersive VCD instrumentation [145–147] and with FTIR instrumentation [148,149]. Depending on the region of interest, the advantages of each type of instrumentation are obvious, though all the commercial VCD instruments are based on FTIR technology. In this special issue Cao et al. [150] present a new method to reduce the effects of linear birefrigerence associated with sample cells, allowing for more accurate and precise VCD measurements.

3.4 Raman scattering spectra for L-alanine

In Fig. 4 we present the simulated Raman scattering spectra at the B3LYP/6-31G* level of theory for the LA20WC, LA20WC plus Onsager continuum solvent model, LA20WC plus PCM continuum solvent model, the LA20WC plus the COSMO continuum solvent model and the experimental spectra. Here we also see that Raman spectra is also affected by the various ways to treat the bulk water molecules. We shall once again use the comparison to the experimental Raman spectra as our method to determine which continuum solvent model is optimum for this purpose. As one can see by comparing the four spectra to the experimental spectra, the simulated spectra all over estimate the band just above 1,500 cm^{-1}. The Onsager appears to do the worst in the relative intensities between 1,600 and 1,800 cm^{-1}. Below 1,500 cm^{-1} all of the four spectra agree quite well with the experimental spectra. To really answer the question of which model is best, one should look at the ROA spectra simulations. The tensors for the ROA spectral simulations are the most time consuming and hence we do not yet have them for the highest level of theory, that is, using the aug-cc-pVDZ basis set for the LA20WC.

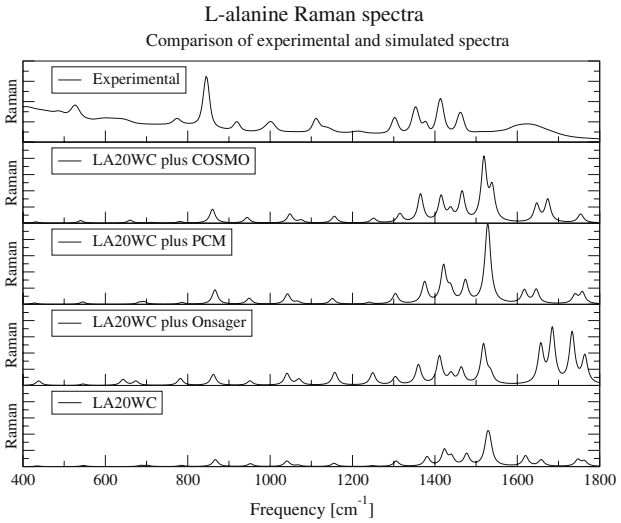

Fig. 4 Comparison of Raman scattering spectra for B3LYP/6-31G* LA20WC, LA20WC + Onsager, LA20WC + PCM and LA20WC + COSMO and experiment

3.5 Raman optical activity spectra for L-alanine

In Fig. 5 we present the newly measured experimental Raman optical activity spectra. In this work we do not present the ROA spectral simulations with the 20 explicit waters and the three continuum models. Here we present the Raman and ROA spectra by using only the PCM continuum model, at the B3LYP/aug-cc-pVDZ level of theory. Surprisingly, when using the aug-cc-pVDZ basis set and the PCM continuum model, the Raman and ROA spectra are in quite good agreement with the experimental spectrum. Using the smaller 6-31G* basis set, the results were not as good, and hence motivated us to include the explicit solvent molecules and also embed the LAZ4WC and LAZ20WC within the continuum solvent models. This may be fortuitous, and hence needs to be documented further. We leave a complete documentation of the PCM and COSMO continuum models for VA, VCD, Raman and ROA for both L-alanine and the alanine dipeptide for a future work, as well as the inclusion of explicit water molecules and the hybrid model.

To simulate the ROA spectra for the LA20WC requires 73 times 6, 438 coupled perturbed Kohn Sham solutions for the G' (EDMDP) and A (EDEQP) tensors. By including the 20 water molecules, one has to perform 6 time 60 = 360 calculations of the EDMDP and and EDEQP, which is quite time consuming This is the additional cost beyond the 6 times 13 = 78 calculations of the EDMDP and EDEQP required for the L-alanine. In addition, one would like to see the effects of both the explicit water molecules and the combined model, that is, the 20 water molecules and the continuum model. Clearly to investigate all of these effects systematically, with respect to various basis sets and exchange-correlations functional is beyond the scope of this work.

Hence we have simulated the ROA spectra using only the LA plus four water molecule model at this time.

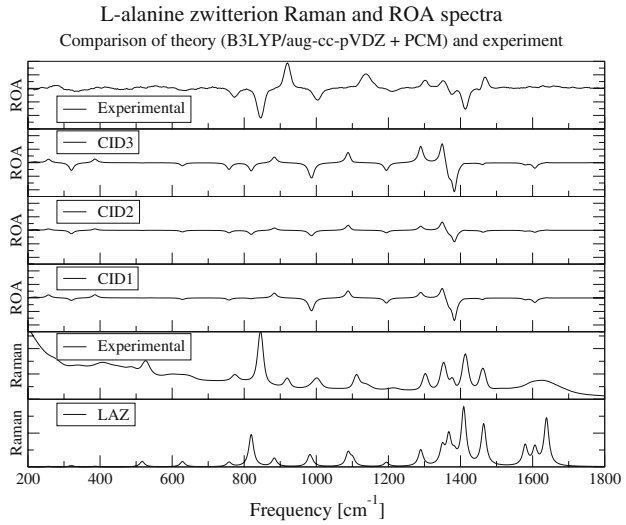

Fig. 5 Comparison of theoretical and experimental Raman and Raman optical activity spectra for LA. B3LYP/aug-cc-pVDZ + PCM level of theory

3.6 Structure of *N*-acetyl L-alanine *N′*-methylamide

The reduced cost of the hybrid models is a big advantage, and for NALANMA, the conformer found to be present in aqueous solution is not even stable on the isolated state potential energy surface and at the Onsager continuum model. This is what motivated us to include the explicit water molecules. The optimized NALANMA4WC structure at the B3LYP/PCM level of theory is given in Fig. 6

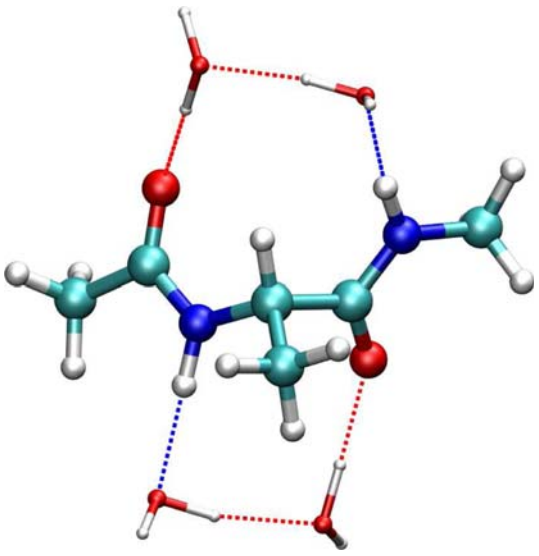

Fig. 6 *N*-acetyl L-alanine *N′*-methyl amide plus four water molecules optimized structure at B3LYP/aug-cc-pVDZ + PCM continuum solvent model

3.7 Vibrational absorption and vibrational circular dichroism for NALANMA

The simulated VA and VCD spectra for the NALANMA plus four water molecule complex with and without the explicit water molecules included in the vibrational analysis are presented in Fig. 7 at the B3LYP/aug-cc-pVDZ plus CPCM (COSMO) continuum model and Fig. 8 at the B3PW91/aug-cc-pVDZ plus CPCM continuum model. Here one can see which regions (modes) of (in) the VA and VCD spectra are affected by the explicit water molecules. In addition, one can see which regions where there is overlap between water modes and those of NALANMA and in addition which regions the modes appear which are due to the hydrogen bonding interactions. For each water molecules interacting with NALANMA one introduces nine internal coordinates, three due to the normal modes of the water molecule and six due to the relative motion of the NALANMA relative to the water molecule. If there were no interactions between NALANMA and the water molecule, these modes would have zero frequency. Hence they give information on the interactions. The information is embedded in the frequencies and VA and VCD intensities. To date this information has been underutilized in both force field parametrization, but also in testing various exchange correlation functionals. Here one can use this information to test how well various exchange correlation functional agree with each other, but also with experimentally measured vibrational frequencies, VA and VCD intensities. In this work, we present out VA and VCD spectral simulations using the B3LYP and B3PW91 functionals, which have been seen to show very similar results for nonpolar molecules in nonpolar solvents. There has been to date very little systematic comparison for polar molecules in polar solvents.

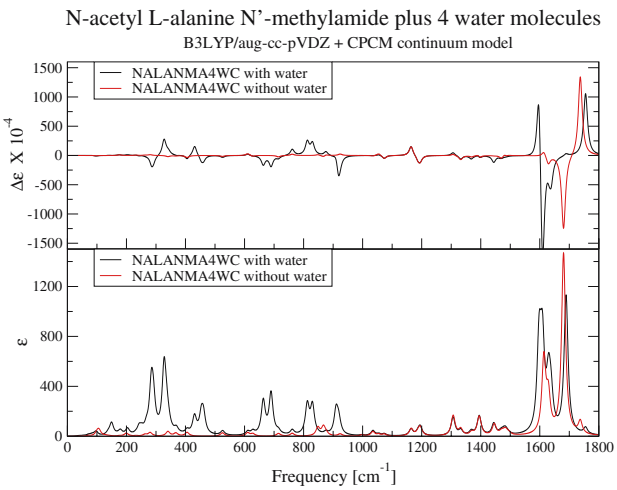

Fig. 7 Comparison of theoretical VA and VCD spectra for NALANMA. B3LYP/aug-cc-pVDZ plus CPCM level of theory with and without explicit water subtraction.

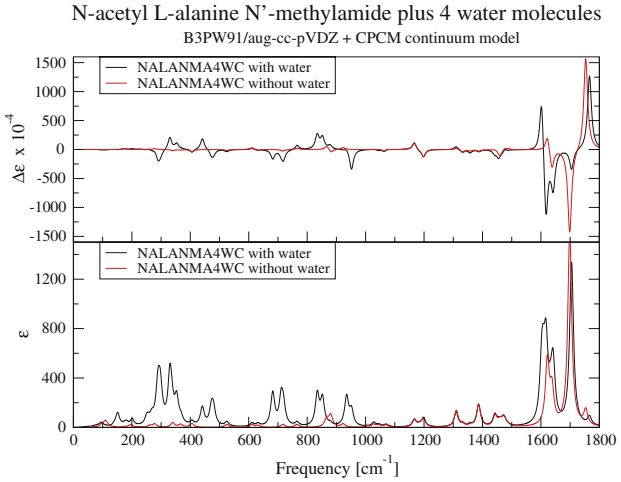

Fig. 8 Comparison of theoretical VA and VCD spectra for NALANMA. B3PW91/aug-cc-pVDZ plus CPCM level of theory with and without explicit water subtraction

3.8 Raman and Raman optical activity spectra for NALANMA

The Raman and ROA spectra along with the experimental spectra for NALANMA are presented in Fig. 9. Clearly the inclusion of explicit water molecules is necessary for NALANMA. Here we have simulated the spectra using the hybrid model, using the explicit solvent model to treat the four water molecules which have been previously shown to be important to stabilize the P_π conformer.

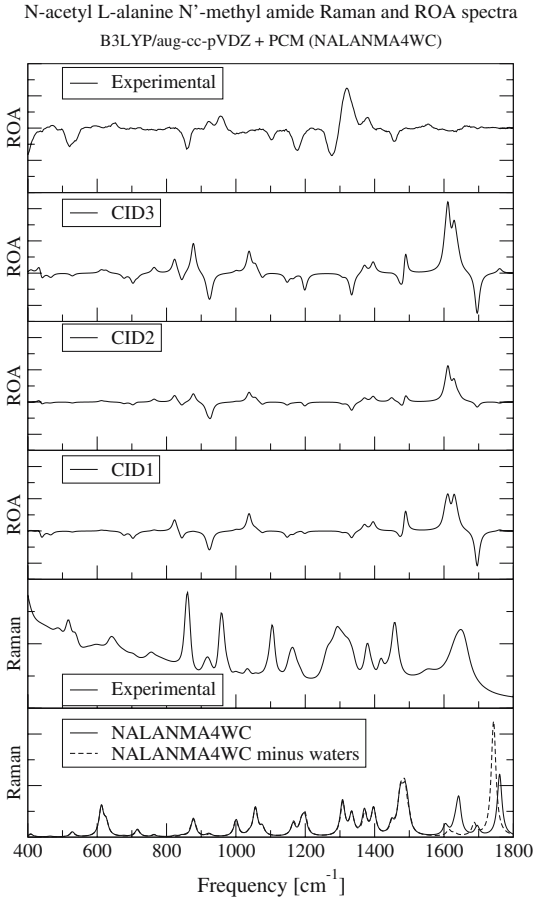

Fig. 9 Comparison of theoretical and experimental Raman and Raman optical activity spectra for NALANMA. B3LYP/aug-cc-pVDZ + PCM level of theory

4 Discussion and conclusions

As one can see from our new VA, VCD, and Raman spectral simulations the effect of the implicit continuum model, be it Onsager, PCM or COSMO still has a relatively large effect on the VA, VCD and Raman spectral simulations, especially in the NH stretch region. Hence the best way to evaluate which model is best is to compare the spectral simulations to our newly reported experimental VA, VCD and Raman scattering spectra. In Table 2 we present the definition of the internal coordinates which we have used for the potential energy distributions (PEDs). The PEDs can be used to assign the vibrational modes. This is also seen in Table 3 where one can see the assignment of the bands in the NH and CH stretch region are not the same. This can also be seen in the NH bond lengths reported in Table 1.

In addition to being used for conformational analysis, VCD can be used to determine the absolute configuration of small chiral molecules [151–156], many of which are ligands and have been found to bind to proteins. Hence the changes in the VCD spectra can also be used to monitor changes in both conformation and absolute configuration. Some drug molecules have been shown to racemize in the body, and hence it is important to know if the drug racemizes before it reaches its target. A classical example is thalidomide, which was given to pregnant women in Europe, Canada and Australia and caused birth defects [157], but was not approved by the FDA in the USA due to concerns by Frances Kelsey at the FDA. This was thought to be due to the drug not being given as an enantiomerically pure form. Subsequently it has been hypothesized that even if it had been given in the enantiomerically pure form (only one enantiomer), it would have still caused problems due to it being racemized in the body.

In addition to using vibrational spectroscopy to monitor changes in conformation, hydrogen bonding and function, other techniques are also complementary, for example, NMR [158] and vibronic spectroscopy [159]. In addition to the analysis of the vibrational frequencies and VA, VCD, Raman and ROA intensities, one can analyze the so called potential energy distributions (PEDs) as we have done here, but also using a decomposition method developed by Hug and Fedorovsky [160] which is presented in this special issue. Here

Table 2 Internal coordinates for the LA + $4H_2O$ molecule for the F' structure

Coord.	Definition	Description[a]	Coord.	Definition	Description[a]
R_1	$\Delta r_{1,2}$	H_1-N_2 s	R_{35}	$\Delta r_{14,16}$	$O_{14}-H_{16}$ s
R_2	$\Delta r_{12,2}$	$H_{12}-N_2$ s	R_{36}	$\Delta\theta_{15,14,16}$	$H_{15}-O_{14}-H_{16}$ b
R_3	$\Delta r_{13,2}$	$H_{13}-N_2$ s	R_{37}	$\Delta r_{17,18}$	$O_{18}-H_{17}$ s
R_4	$\Delta r_{9,7}$	H_9-C_7 s	R_{38}	$\Delta r_{18,19}$	$O_{18}-H_{19}$ s
R_5	$\Delta r_{10,7}$	$H_{10}-C_7$ s	R_{39}	$\Delta\theta_{17,18,19}$	$H_{17}-O_{18}-H_{19}$ b
R_6	$\Delta r_{11,7}$	$H_{11}-C_7$ s	R_{40}	$\Delta r_{20,21}$	$O_{20}-H_{21}$ s
R_7	$\Delta r_{8,3}$	H_8-C_3 s	R_{41}	$\Delta r_{20,22}$	$O_{20}-H_{22}$ s
R_8	$\Delta r_{5,4}$	O_5-C_4 s	R_{42}	$\Delta\theta_{21,20,22}$	$H_{21}-O_{20}-H_{22}$ b
R_9	$\Delta r_{6,4}$	O_6-C_4 s	R_{43}	$\Delta r_{23,24}$	$O_{23}-H_{24}$ s
R_{10}	$\Delta r_{2,3}$	N_2-C_3 s	R_{44}	$\Delta r_{23,25}$	$O_{23}-H_{25}$ s
R_{11}	$\Delta r_{3,4}$	C_3-C_4 s	R_{45}	$\Delta\theta_{24,23,25}$	$H_{24}-O_{23}-H_{25}$ b
R_{12}	$\Delta r_{3,7}$	C_3-C_7 s	R_{46}	$\Delta r_{1,14}$	$H_1\ldots O_{14}$ s
R_{13}	$(1/\sqrt{6})(\Delta\theta_{13,2,1}+\Delta\theta_{13,2,12}+\Delta\theta_{1,2,12}-\Delta\theta_{13,2,3}-\Delta\theta_{1,2,3}-\Delta\theta_{12,2,3})$	$N_2H_{1,12,13}C_3$ sd	R_{47}	$\Delta\theta_{2,1,14}$	$N_2-H_1\ldots O_{14}$ b
			R_{48}	$\Delta\theta_{1,14,15}$	$H_1\ldots O_{14}-H_{15}$ b
R_{14}	$(1/\sqrt{6})(2\Delta\theta_{13,2,1}-\Delta\theta_{13,2,12}-\Delta\theta_{1,2,12})$	$N_2H_{1,12,13}$ asd	R_{49}	$\Delta\theta 1, 14, 16$	$H_1\ldots O_{14}-H_{16}$ b
R_{15}	$(1/\sqrt{2})(\Delta\theta_{13,2,12}-\Delta\theta_{1,2,12})$	$N_2H_{1,12,13}$ asd	R_{50}	$\tau_{1,14}$	H_1-O_{14} tor
R_{16}	$(1/\sqrt{6})(2\Delta\theta_{13,2,3}-\Delta\theta_{13,2,12}-\Delta\theta_{1,2,12})$	$N_2H_{1,12,13}C_3$ r	R_{51}	$\tau_{2,1}$	N_2-H_1 tor
R_{17}	$(1/\sqrt{2})(\Delta\theta_{1,2,3}-\Delta\theta_{12,2,3})$	$N_2H_{1,12,13}C_3$ r	R_{52}	$\Delta r_{6,17}$	O_6-H_{17} s
R_{18}	$(1/\sqrt{6})(\Delta\theta_{9,7,11}+\Delta\theta_{9,7,10}+\Delta\theta_{11,7,10}-\Delta\theta_{9,7,3}-\Delta\theta_{11,7,3}-\Delta\theta_{10,7,3})$	$C_7H_{9,10,11}C_3$ sd	R_{53}	$\Delta\theta_{4,6,17}$	$C_4-O_6\ldots H_{17}$ b
			R_{54}	$\Delta\theta_{6,17,18}$	$O_6\ldots H_{17}-O_{18}$ b
R_{19}	$(1/\sqrt{6})(2\Delta\theta_{9,7,11}-\Delta\theta_{9,7,10}-\Delta\theta_{11,7,10})$	$C_7H_{9,10,11}$ asd	R_{55}	$\tau_{4,6}$	C_4-O_6 tor
R_{20}	$(1/\sqrt{2})(\Delta\theta_{9,7,10}-\Delta\theta_{11,7,10})$	$C_7H_{9,10,11}$ asd	R_{56}	$\tau_{6,17}$	O_6-H_{17} tor
R_{21}	$(1/\sqrt{6})(2\Delta\theta_{9,7,3}-\Delta\theta_{11,7,3}-\Delta\theta_{10,7,3})$	$C_7H_{9,10,11}C_7$ r	R_{57}	$\tau_{17,18}$	$H_{17}-O_{18}$ b
R_{22}	$(1/\sqrt{2})(\Delta\theta_{11,7,3}-\Delta\theta_{10,7,3})$	$C_7H_{10,11}C_3$ r	R_{58}	$\Delta r_{5,21}$	$O_5\ldots H_{21}$ s
R_{23}	$(1/\sqrt{6})(2\Delta\theta_{8,3,2}-\Delta\theta_{8,3,4}-\Delta\theta_{8,3,7})$	$H_8-C_3-N_2$ b	R_{59}	$\Delta\theta_{4,5,21}$	$C_4-O_5\ldots H_{21}$ b
R_{24}	$(1/\sqrt{2})(\Delta\theta_{8,3,4}-\Delta\theta_{8,3,7})$	$H_8-C_3-C_4$ b	R_{60}	$\Delta\theta_{5,21,20}$	$O_5\ldots H_{21}-O_{20}$ b
R_{25}	$(1/\sqrt{18})(4\Delta\theta_{4,3,2}+\Delta\theta_{4,3,7}+\Delta\theta_{2,3,7})$	$O_5-C_4-C_3$ b	R_{61}	$\tau_{4,5}$	C_4-O_5 tor
R_{26}	$(1/\sqrt{18})(4\Delta\theta_{4,3,7}+\Delta\theta_{4,3,2}+\Delta\theta_{2,3,7})$	$O_6-C_4-C_3$ b	R_{62}	$\tau_{5,21}$	O_5-H_{21} tor
R_{27}	$(1/\sqrt{18})(4\Delta\theta_{2,3,7}+\Delta\theta_{4,3,2}+\Delta\theta_{4,3,7})$	$C_7-C_3-N_2$ b	R_{63}	$\tau_{21,20}$	$H_{21}-O_{20}$ tor
R_{28}	$(1/\sqrt{6})(2\Delta\theta_{5,4,6}-\Delta\theta_{3,4,5}-\Delta\theta_{3,4,6})$	$C_7-C_3-C_4$ b	R_{64}	$\Delta r_{13,23}$	$H_{13}\ldots O_{23}$ s
R_{29}	$(1/\sqrt{2})(\Delta\theta_{3,4,5}-\Delta\theta_{3,4,6})$	$N_2-C_3-C_4$ b	R_{65}	$\Delta\theta_{2,13,23}$	$N_2-H_{13}\ldots O_{23}$ b
R_{30}	$\tau_{4,5}$	$C_3-C_4-O_5-O_6$ opw	R_{66}	$\Delta\theta_{13,23,24}$	$H_{13}\ldots O_{23}-H_{24}$ b
R_{31}	$\tau_{2,3}$	$H_1-N_2-C_3-C_4$ tor	R_{67}	$\Delta\theta_{13,23,25}$	$H_{13}\ldots O_{23}-H_{25}$ b
R_{32}	$\tau_{3,4}$	$N_2-C_3-C_4-O_6$ tor	R_{68}	$\tau_{13,23}$	$H_{13}-O_{23}$ tor
R_{33}	$\tau_{7,3}$	$H_9-C_7-C_3-N_2$ tor	R_{69}	$\tau_{2,13}$	$H_{13}-O_{23}$ tor
R_{34}	$\Delta r_{14,15}$	$O_{14}-H_{15}$ s			

Atom numbering corresponds to those in Fig. 1 reference [2]

[a] Classification of coordinates:

tor torsion, *s* stretch, (a) *sd* (a)symmetric deformation, *r* rocking, *b* bend, *opw* out of plane wagging

one is able to assign the experimental observables (frequencies and VA, VCD, Raman and ROA intensities) to specific functional groups in the molecule. This is very important for molecules with multiple chiral centers, for example, aframodial, which has four chiral centers [156]. The method of Hug and Fedorovsky complements the method of PEDs used by Jalkanen et al. [161] in this special issue where they document the use of various sets of internal coordinates for not only the assignment of the normal modes, but also in terms of scaling force fields and transferability. The use of symmetric molecules to determine scale factors has been documented for both ethylene oxide [77] and 2-oxetanone [162].

The question of how many solvent molecules are in the first hydration shell of water has been investigated. Here

Table 3 Assignments based on potential energy distributions for LA in H_2O

F′	Assgn	F‴	Assgn	Barron	Assgn	Yu	Assgn	I	Assgn	II	Assgn	Exptl	Assgn
$\nu(cm^{-1})$	PED	$\nu(cm^{-1})$	PED	$\nu(cm^{-1})$	PED	$\nu(cm^{-1})$	PED	$\nu(cm^{-1})$	PED	$\nu(cm^{-1})$	PED	$\nu(cm^{-1})$	PED
3,164	$R_{5,6}$	3,161	$R_{5,6}$	3,809	$R_{3,1}$	3,712	R_1	3,266.	R_2	3,176.	$R_{5,6}$	3,080	$\nu^a_{NH_3^+}$
3,142	$R_{2,1}$	3,138	$R_{6,4}$	3,727	$R_{1,3}$	3,689	$R_{3,2}$	3,205.	$R_{6,5}$	3,151.	$R_{6,4}$	3,060	$\nu^a_{NH_3^+}$
3,137	$R_{1,3}$	3,103	R_3	3,334	R_5	3,599	$R_{2,3,1}$	3,176.	$R_{5,4,6}$	3,089.	R_7	3,020	$\nu^s_{NH_3^+}$
3,135	$R_{6,4}$	3,086	R_7	3,295	R_7	3,326	$R_{5,6}$	3,124.	R_7	3,080.	$R_{4,6,5}$	3,003	$\nu^a_{CH_3}$
3,113	$R_{3,2,1,7}$	3,066	$R_{4,6,5}$	3258	$R_{4,6}$	3292	$R_{6,4,7}$	3,096.	$R_{4,5,6}$	2,988.	R_2	2,993	$\nu^a_{CH_3}$
3,093	R_7	3,026	R_2	3,204	$R_{6,4}$	3,272	$R_{7,6}$	2,952.	R_1	2,956.	$R_{3,1}$	2,962	ν_{C*H}
3,064	$R_{4,6,5}$	2,990	R_1	2,813	R_2	3,214	$R_{4,6,5}$	2,831.	R_3	2,944.	$R_{1,3}$	2,949	$\nu^s_{CH_3}$
1,759	$R_{14,15}$	1,778	R_{14}	1,996	$R_{8,9}$	1,877	$R_{9,8}$	1,758.	$R_{15,17}$	1,756.	$R_{14,31}$	1,645	$\delta^a_{NH_3^+}$
1,750	$R_{15,14}$	1,766	R_{15}	1,822	R_{15}	1,836	$R_{14,15}$	1,740.	$R_{14,31}$	1,753.	$R_{15,17}$	1,625	$\delta^a_{NH_3^+}$
1,695	$R_{8,9}$	1,678	$R_{13,9,8}$	1,790	$R_{14,13}$	1,802	$R_{14,15}$	1646.	$R_{9,8}$	1,674.	$R_{9,13,8}$	1,607	$\nu^a_{CO_2^-}$
1,635	R_{13}	1,653	$R_{13,9,8}$	1,641	R_{19}	1,652	R_{13}	1,617.	R_{13}	1,647.	$R_{13,9}$	1498	$\delta^s_{NH_3^+}$
1,536	$R_{19,20}$	1,536	$R_{19,20}$	1,639	R_{20}	1,642	R_{19}	1,530.	$R_{20,19}$	1,539.	$R_{19,20}$	1,459	$\delta^a_{CH_3}$
1,529	$R_{20,19}$	1,529	$R_{20,19}$	1,568	R_{18}	1,636	R_{20}	1,527.	$R_{19,33,21}$	1,519.	$R_{19,33,21}$	1,459	$\delta^a_{CH_3}$
1,441	R_{18}	1,456	$R_{18,9,11,8}$	1,523	$R_{13,9,8,23}$	1,578	R_{18}	1,474.	$R_{19,18}$	1,466.	$R_{19,23,18}$	1,410	$\nu^s_{CO_2^-}$
1,416	$R_{23,18,17}$	1,422	$R_{18,23}$	1,501	$R_{23,9}$	1,542	$R_{18,8,9,11}$	1,438.	$R_{18,23}$	1,438.	$R_{18,23}$	1,375	$\delta^s_{CH_3}$
1,390	$R_{9,11,16}$	1,394	$R_{23,8}$	1,447	$R_{24,13,11}$	1,502	R_{23}	1,421.	$R_{18,23,8}$	1,415.	$R_{8,17,24,23}$	1,351	δ_{C*H}
1,350	$R_{24,9}$	1,351	$R_{24,16}$	1,395	$R_{13,9,14}$	1,452	R_{24}	1,375.	$R_{17,24,19,8}$	1,365.	$R_{8,17,24}$	1,301	δ_{C*H}
1,290	$R_{16,22,23,24}$	1,274	$R_{16,22}$	1,314	$R_{22,17,12,27}$	1,317	$R_{22,16,27,12}$	1,394.	$R_{17,22,24,16}$	1,315.	$R_{22,17,16,24}$	1220	$\zeta_{NH_3^+}$
1,213	$R_{17,24,23}$	1,207	$R_{17,24}$	1,205	$R_{21,24,16}$	1,222	$R_{21,24,17}$	1,240.	$R_{16,17,22,24}$	1,251.	$R_{16,17,24}$	1145	$\zeta_{NH_3^+}$
1,133	$R_{21,10,12}$	1,143	$R_{21,10,12}$	1,164	$R_{16,25,10,12}$	1,186	$R_{10,12,17,21,16}$	1151.	$R_{10,21,19}$	1156.	$R_{10,21,19}$	1110	ν^a_{CCN}
1,062	$R_{22,16,12}$	1,057	$R_{22,16,12}$	1,080	$R_{16,12,21}$	1,061	$R_{17,22}$	1,067.	$R_{22,12,16}$	1,075.	$R_{22,12}$	1001	$\nu_{CC(O_2)}$
1,028	$R_{12,21,10}$	1,030	$R_{12,21,10}$	1,060	$R_{17,22}$	1,048	$R_{16,22}$	1,042.	$R_{21,12,33,10}$	1,048.	$R_{21,12,10}$	995	ζ_{CH_3}
918	$R_{10,11,22}$	938	$R_{10,11,22}$	942	$R_{11,28,10}$	970	$R_{11,10,28}$	949.	$R_{21,22,10,11}$	944.	$R_{21,22,10,11}$	922	ζ_{CH_3}
840	$R_{28,10,11}$	854	$R_{28,10,11,12}$	881	$R_{10,28}$	894	$R_{10,30,28}$	866.	$R_{22,28,33}$	860.	$R_{22,28,33,11}$	850	ν^s_{CCN}
775	$R_{30,28,26}$	771	$R_{30,26}$	838	$R_{30,28}$	844	$R_{30,28}$	786.	R_{30}	781.	$R_{30,33}$	775	$\gamma_{CO_2^-}$
635	R_{31}	704	R_{31}	681	$R_{25,11,29,30}$	640	$R_{11,28,25,30}$	694.	$R_{33,31,21}$	712.	$R_{31,22}$	640	$\delta_{CO_2^-}$

Table 3 continued

F′	Assgn	F‴	Assgn	Barron	Assgn	Yu	Assgn	I	Assgn	II	Assgn	Exptl	Assgn
$\nu(cm^{-1})$	PED	$\nu(cm^{-1})$	PED	$\nu(cm^{-1})$	PED	$\nu(cm^{-1})$	PED	$\nu(cm^{-1})$	PED	$\nu(cm^{-1})$	PED	$\nu(cm^{-1})$	PED
625	$R_{25,28,11,30}$	632	$R_{25,28,11,30,29}$	562	$R_{29,11,10}$	536	$R_{29,10,11}$	683.	$R_{31,22,33}$	660.	$R_{33,25,28,22}$	527	$\zeta_{CO_2^-}$
528	$R_{29,11,25,27,10}$	533	$R_{29,27,11,25}$	413	R_{27}	426	$R_{27,26}$	545.	$R_{29,27,21,22}$	540.	$R_{29,27,22,21}$	477	$\tau_{NH_3^+}$
432	R_{27}	436	R_{27}	352	$R_{25,2,29}$	330	$R_{25,26}$	428.	$R_{27,21}$	431.	$R_{27,21,22,32}$	399	δ_{skel}
355	$R_{25,29,26}$	363	$R_{25,29,26}$	303	$R_{31,15}$	275	$R_{26,29,25}$	353.	$R_{33,22}$	346.	$R_{33,22}$	296	τ_{CH_3}
290	$R_{26,29}$	291	$R_{26,29,25}$	275	$R_{26,29,33}$	254	$R_{33,26}$	280.	$R_{26,21,33,30}$	284.	$R_{26,22,21,32}$	283	δ_{skel}
264	$R_{33,26}$	261	$R_{33,26}$	255	$R_{33,26}$	138	$R_{31,16}$	206.	$R_{33,22}$	248.	$R_{33,22}$	219	δ_{skel}
170	R_{32}	152	R_{32}	54	$R_{31,32}$	84	$R_{32,31}$	184.	$R_{33,22}$	200.	$R_{33,22}$	184	$\tau_{CO_2^-}$

F′ B3LYP/6-31G* + 4H_2O +Onsager from [1]
F‴ B3LYP/6-31G* + 9H_2O + Onsager from [2]
Barron RHF/6-31G* from [134]
Yu′ RHF/6-31G* + Onsager from [142]
I B3LYP/6-31G* + 20H_2O + PCM
II B3LYP/6-31G* + 20H_2O + COSMO
Exptl LA in H_2O/solid from [116,134,142,182,183]
F′ (PED) B3LYP/6-31G* + 4H_2O + Onsager this work
F‴ (PED) B3LYP/6-31G* + 9H_2O + Onsager this work
Barron (PED) RHF/6-31G* this work
Yu′ (PED) RHF/6-31G* + Onsager this work
I (PED) B3LYP/6-31G* + 20H_2O + PCM this work
II (PED) B3LYP/6-31G* + 20H_2O + COSMO this work
Exptl Assignment based on group frequencies and isotopic data [182]

we have increased the number of water molecules from 4 [1,21] and 9 [2,26] which we have used in our previous studies to 20. Our definition is the number of water molecules which are necessary to completely encapsulate the LA zwitterion. An experimental determination of the hydration number of glycine has also recently been reported [163]. In their work they have utilized calorimetric methods and determined that the hydration number or glycine is 7 for the zwitterionic form. In addition to this calorimetric method, low temperature matrix isolation Fourier transform infrared techniques have also been used [164] in addition to ATR studies [165]. NMR studies of the hydration of biological molecules have also been undertaken [166]. The effects of hydration, other hydrogen bonding interactions and hydrophobic packing interactions have been observed to affect and distort the helix structures of proteins from their ideal 3.6_{13} and 3_{10} structures [167] and also been shown to important in both protein folding, unfolding and refolding (after removal of denaturant, lower temperature or removal of other perturbation which caused the unfolding or denaturing) [168]. As many molecular diseases are caused by misfolding of proteins, it is fundamental that we can understand not only the effects which can cause misfolding or denaturing if we wish to prevent these occurrences, but we also need to understand the possible ways to refold, in the event that the process is reversible. The difference between irreversible and reversible misfolding and denaturing is not obvious and clear, and the class of proteins which can be reversibly refolded does not appear to be large. In many cases other proteins may be necessary to help the protein refold (and in some cases to even fold initially), the so called chaperon proteins. In the case of the damaged (denatured) DNA, the photolyase protein have been shown to be able to initiate repair, but require blue light, in a so called photoinitiated repair process [169–173].

For the case of NALANMA the early vibrational analyzes used HF/4-21G force fields which needed to be scaled [174, 175]. We extended this work by using the RHF/6-31G* [23] and subsequently B3LYP/6-31G* force fields. In our works we did not scale the force fields, as by doing so one masks the systematic errors and one then loses sights of both the errors and approximations made. Subsequently the treatment of the molecule was also undertaken, initially at the scale HF/4-21G level [176] and then subsequently by us at the B3LYP/6-31G* level of theory. The initial studies were important in documenting the structure and vibrational spectra of NALANMA in the isolated state, in nonpolar solvents, in inert gas matrices (so called matrix isolation studies) and finally in the crystal. When one measured the spectra of NALANMA in aqueous solution one noticed large changes in the spectra. The early works which did not include the explicit treatment of solvent [23] were not able to fully interpret the spectra in aqueous solution, but surprisingly the spectra of a transition state species gave the best agreement with the experimentally observed spectra. This motivated us to use explicit solvent models, implicit solvent models and finally a combination of the two, where we used an explicit solvent treatment to treat the water molecules which had specific and directionally oriented interactions which were responsible for stabilizing species not stable in the isolated state or gas phase potential energy surface (PES) [3,22,177], and an implicit water model to treat the effects due to the bulk water.

This NALANMA4WC was subsequently sent to NMR spectroscopists who were then able to interpret the NMR spectra of this molecule, which had previously not been able to be interpreted using the conformers which are only stable on the isolated state PES [178,179]. In this work using B3LYP/aug-cc-pVDZ and B3PW91/aug-cc-pVDZ levels of theory we have further confirmed and established that NALANMA with four explicit water molecules (NALAN MA4WC) is a stable complex which is the global minimum and that the VA, VCD, Raman and ROA spectra are in good agreement with those experimentally measured. In addition, we have embedded the NALANMA4WC within three continuum models: the Onsager, PCM and CPCM models which have treated the effects due to bulk water molecules. Hence there should no longer be any doubt that the combination of explicit and implicit solvent models using hybrid XC functionals in DFT with relatively large basis sets (aug-cc-pVDZ or larger) are needed to accurately treat the VA, VCD, Raman and ROA spectra. By combining these latest theoretical and experimental methods one now has the opportunity to fully interpret and utilize the VA, VCD, Raman and ROA spectra of biological molecules in aqueous solution. The theory of VCD developed by Stephens [99,101] and Buckingham [106] and the theory of ROA developed by Barron and Buckingham [129] and Nafie [180] for isolated molecules has now been extended to condensed matter physics, aqueous solution, in addition to the previous isolated state, inert gas matrices and nonpolar solvents. With the commercial availability of Chiral FTIR and Chiral Raman instrumentation [151] as well as both commercial and academic codes which can simulate the spectra measured the chiral vibrational spectroscopies have now become tools which to date have been untapped. We hope this mini review and our updated original work on LA and NALANMA which have been used to understand fully the structural changes in these molecules as one changes the phase/environment, will serve as a basis for other groups to use these techniques in their works in structural biology, physical biochemistry, molecular biophysics and quantum nanobiology. Like their complementary tools, X-ray and neutron diffraction and NMR, vibrational spectroscopy once again is taking its place a very powerful tool in the nano-, quantum- and molecular-based sciences.

Acknowledgments KJJ would like to acknowledge the Western Australia government's Premier Fellowship program for providing financial support and the iVEC Supercomputer Centre of Western Australia and the APAC National Supercomputer in Canberra for providing computational facilities. KJJ would also like to thank Alexandra Wassileva for her work on the literature review of the experimental spectra on both L-alanine and NALANMA at the German Cancer Research Centre in Heidelberg, Germany. We would like to thank Dr. S.K. Wolff for careful reading of the manuscript and feedback which was incorporated to make the work more clear and concise.

References

1. Tajkhorshid E, Jalkanen KJ, Suhai S (1998) J Phys Chem B 102: 5899
2. Frimand K, Jalkanen KJ, Bohr HG, Suhai S (2000) Chem Phys 255:165
3. Han W-G, Jalkanen KJ, Elstner M, Suhai S (1998) J Phys Chem B 102:2587
4. Perkins SJ (2001) Biophys Chem 93:129
5. Gerstein M, Chothia C (1996) Proc Natl Acad Sci USA 93:10167
6. Degtyarenko IM, Jalkanen KJ, Gurtovenko AA, Nieminen RM (2007) J Comput Theor Nanosci (accepted in press)
7. Blanch EW, Hecht L, Barron LD (1999) Protein Sci 8:1362
8. Roberts G-ML (1990) Ph.D. thesis, The City University of New York (Hunter College), New York
9. Roberts G-ML, Diem M (1987) In: Schmid ED, Schneider FW, Siebert F (eds) Spectroscopy of biological molecules new advances. Proceedings of the Second European conference of the spectroscopy of biological molecules, Freiburg, West Germany, 1988. Wiley, New York pp 77–79
10. Madison V, Kopple KD (1980) J Am Chem Soc 102:4855
11. Maxfield FR, Leach SJ, Stimson ER, Powers SP, Scheraga HA (1979) Biopolymers 18:2507
12. Grenie Y, Avignon M, Garribou-Lagrange C (1975) J Mol Struct 24:293
13. Mattice WL (1974) Biopolymers 13:169
14. Avignon M, Garrigou-Lagrange C, Bothorel P (1973) Biopolymers 12:1651
15. Cann JR (1972) Biochemistry 11:2654
16. Koyama Y, Shimanouchi T, Sato M, Tatsuno T (1971) Biopolymers 10:1059
17. Avignon M, Houng PV (1970) Biopolymers 9:427
18. Avignon M, Huong PV, Lascombe J, Marraud M, Neel J (1969) Biopolymers 8:69
19. Mizushima S-I, Shimanouchi T, Tsuboi M, Sugita T, Kurosaki K, Mataga N, Souda R (1952) J Am Chem Soc 74:4639
20. Blanco S, Lesarri A, Lopez JC, Alonso JL (2004) J Am Chem Soc 126:11675
21. Jalkanen KJ, Bohr HG, Suhai S (1997) In: Suhai S (ed) Proceedings of the international symposium on theoretical and computational genome research. Plenum Press, New York pp 255–277
22. Jalkanen KJ, Suhai S (1996) Chem Phys 208:81
23. Deng Z, Polavarapu PL, Ford SJ, Hecht L, Barron LD, Ewig CS, Jalkanen KJ (1996) J Phys Chem 100:2025
24. Baker MV, Kraatz H-B, Quail JW (2001) New J Chem 25:427
25. Bohr HG, Jalkanen KJ, Frimand K, Elstner M, Suhai S (1999) Chem Phys 246:13
26. Jalkanen KJ, Nieminen RM, Frimand K, Bohr J, Bohr H, Wade RC, Tajkhorshid E, Suhai S (2001) Chem Phys 265:125
27. Knapp-Mohammady M, Jalkanen KJ, Nardi F, Wade RC, Suhai S (1999) Chem Phys 240:63
28. Jalkanen KJ, Nieminen RM, Knapp-Mohammady M, Suhai S (2003) Int J Quantum Chem 92:239
29. Jalkanen KJ (2003) J Phys Condens Matter 15:S18230
30. Jalkanen KJ, Elstner M, Suhai S (2004) J Mol Struct (Theochem) 675:61
31. Deplazes E, van Bronswijk B, Zhu F, Barron LD, Ma S, Nafie LA, Jalkanen KJ (2007) Theor Chem Acc doi:10.1007/s00214-007-0276-8
32. Bohr H, Frimand K, Jalkanen KJ, Nieminen RM, Suhai S (2001) Phys Rev E 64:021905
33. Bohr H, Røgen P, Jalkanen KJ (2001) Comput Chem 26:65
34. Barron LD, Zhu F, Hecht L (2006) Vib Spectrosc 42:15
35. Barron LD, Hecht L, Blanch EW, Bell AF (2000) Prog Biophys Mol Biol 73:1
36. Ramnarayan K, Bohr HG, Jalkanen KJ (2007) Theor Chem Acc doi:10.1007/s00214-007-0285-7
37. Venyaminov SY, Kalnin NN (1990) Biopolymers 30:1243
38. Venyaminov SY, Kalnin NN (1990) Biopolymers 30:1259
39. Kalnin NN, Baikalov IA, Venyaminov SY (1990) Biopolymers 30:1273
40. Baumruk V, Pancoska P, Keiderling TA (1996) J Mol Biol 259:774
41. Iftimie R, Tuckerman ME (2006) Angew Chem Int Ed 45:1144
42. Steiner T (2002) Angew Chem Int Ed 41:48
43. Gorelsky SI, Solomon EI (2007) Theor Chem Acc doi:10.1007/s00214-007–270-1
44. Gorelsky SI, Solomon EI (2007) Theor Chem Acc doi:10.1007/s00214-007-0289-3
45. Venyaminov SY, Baikalov IA, Wu C-SC, Yang JT (1991) Anal Biochem 198:250
46. Jalkanen KJ, Jürgensen VW, Claussen A, Jensen GM, Rahim A, Wade RC, Nardi F, Jung C, Nieminen RM, Degtyarenko IM, Herrmann F, Knapp-Mohammady M, Niehaus T, Frimand K, Suhai S (2006) Int J Quantum Chem 106:1160
47. Malkin VG, Malkina OL, Eriksson LA, Salahub DR (1995) The calculation of NMR and ESR spectroscopy parameters using density functional theory. In: Seminario JM, Politzer P (eds) Modern density functional theory: a tool for chemistry, vol 2. Elsevier Science B.V., pp 273–347
48. Eker F, Cao X, Nafie L, Huang Q, Schweitzer-Stenner R (2–3) J Phys Chem B 107:358
49. Motta A, Reches M, Pappalardo L, Andreotti G, Gazit E (2005) Biochemistry 44:14178
50. Nilsson A, Ogasawara H, Cavalleri M, Nordlund D, Nyberg M, Wernet Ph, Pettersson LGM (2005) J Chem Phys 122:154505
51. Russell AJ, Spackman MA (2000) Mol Phys 98:855
52. Russell AJ, Spackman MA (2000) Mol Phys 98:867
53. Herrmann C, Reiher M (2007) Top Curr Chem 268:85
54. Zhu F, Issacs NW, Hecht L, Tranter GE, Barron LD (2006) Chirality 18:103
55. Barron LD (2006) Curr Opin Struct Biol 16:638
56. Barron LD, Hecht L, McColl IH, Blanch EW (2004) Mol Phys 102:731
57. Bouř P (2004) J Chem Phys 121:7545
58. Mahoney MW, Jorgensen WL (2000) J Chem Phys 112:8910
59. Cabral do Couto P, Estácio SG, Costa Cabral BJ (2005) J Chem Phys 123:054510
60. Degtyarenko IM, Jalkanen KJ, Gurtovenko AA, Nieminen RM (2007) J Phys Chem B 111:4227
61. Onsager L (1936) J Am Chem Soc 58:1486
62. Tomasi J, Persico M (1994) Chem Rev 94:2027
63. Klamt A, Schüürmann G (1993) J Chem Soc Perkin Trans 2:799–805
64. Klamt A (1995) J Phys Chem 99:2224
65. Klamt A (1996) J PhysChem 100:3349

66. Klamt A, Jonas V, Bürger T, Lohrenz JCW (1998) J Phys Chem 102:5074
67. Miltner M, Miltner A, Friedl A (2006) Chemie Ingenieur Technik 78:1087
68. Thanki N, Thornton JM, Goodfellow JM (1988) J Mol Biol 202: 637
69. Tomasi J, Mennucci B, Cammi R (2005) Chem Rev 105:2999
70. Orozco M, Luque FJ (2000) Chem Rev 100:4187
71. Cramer CJ, Truhlar DG (1999) Chem Rev 99:2161
72. Lin H, Truhlar DG (2007) Theor Chem Acc 117:185
73. McLain SE, Soper AK, Terry AE, Watts A (2007) J Phys Chem B doi:10.1021/jp068340f
74. Murray CW, Laming GJ, Handy NC, Amos RD (1992) Chem Phys Lett 199:551
75. Johnson BG, Frisch MJ (1993) Chem Phys Lett 216:133
76. van Caillie C, Amos RD (2000) Chem Phys Lett 317:159
77. Lowe MA, Alper JS, Kawiecki RW, Stephens PJ (1986) J Phys Chem 90:41
78. Mirkin NG, Krimm S (1991) J Am Chem Soc 113:9742
79. Williams RW (1992) Biopolymers 32:829
80. Mirkim NG, Krimm S (1996) J Mol Struct 377:219
81. Maple JR, Hwang M-J, Jalkanen KJ, Stockfisch TP, Hagler AT (1998) J Comp Chem 19:430
82. Schellman JA (1975) Chem Rev 75:323
83. Kawiecki RW, Devlin FJ, Stephens PJ, Amos RD (1991) J Phys Chem 95:9817
84. Delgarno A (1959) Proc R Soc Lond Series A Math Phys Sci 251:282
85. Delgarno A (1962) Adv Phys 11:281
86. Delgarno A, Victor GA (1966) Proc Roy Soc Lond Series A Math Phys Sci 291:291
87. Gerratt J, Mills IM (1968) J Chem Phys 49:1719
88. Amos RD (1984) Chem Phys Lett 108:185
89. Hall GG (1951) Proc R Soc Lond Ser A Math Phys Sci 205:541
90. Hall GG (1959) Rep Prog Phys 22:1
91. Roothaan CCJ (1951) Rev Mod Phys 23:69
92. Salek P, Høst S, Thøgersen L, Jørgensen P, Manninen P, Olsen J, Jansik B, Reine S, Pawlowski F, Tellgren E, Helgaker T, Coriani S (2007) J Chem Phys 126:114110
93. te Velde G, Bickelhaupt FM, Baerends EJ, Guerra CF, van Gisbergen SJA, Snijders JG, Ziegler T (2001) J Comp Chem 22:931
94. Wolff SK (2005) Int J Quant Chem 104:645
95. Nicu VP, Neugebauer J, Wolff SK, Baerends EJ (2006) Theor Chem Acc doi:10.1007/s00214-006-0234-x
96. Halls MD, Schlegel HB (1999) J Chem Phys 109:10587
97. Jalkanen KJ, Jürgensen VW, Degtyarenko IM (2006) Adv Quantum Chem 50:91
98. Ghosez P, Gonze X (2000) J Phys Consens Matter 12:9179
99. Stephens PJ (1985) J Phys Chem 89:748
100. Amos RD, Handy NC, Jalkanen KJ, Stephens PJ (1987) Chem Phys Lett 133:21
101. Stephens PJ (1987) J Phys Chem 91:1712
102. Amos RD, Jalkanen KJ, Stephens PJ (1988) J Phys Chem 92:5571
103. Stephens PJ, Jalkanen KJ, Amos RD, Lazzeretti P, Zanasi R (1990) J Phys Chem 94:1811
104. Hunt KLC, Harris RA (1991) J Chem Phys 94:6995
105. Nafie LA, Dukor RK, Freedman TB (2002) Vibrational circular dichroism. In: Chalmers JM, Griffiths PR (eds) Handbook of vibrational spectroscopy. Wiley, Chichester, pp 731–744
106. Buckingham AD, Fowler PW, Galwas PA (1987) J Chem Phys 112:1
107. Barron LD, Buckingham AD (2001) Acc Chem Res 34:781
108. Born M, Huang K (1964) Dynamical theory of crystal Lattices. Oxford University Press, Oxford
109. Mead CA, Moscowitz A (1967) Int J Quant Chem 1:243
110. Jalkanen KJ, Stephens PJ, Amos RD, Handy NC (1988) J Phys Chem 92:1781
111. Hansen AE, Stephens PJ, Bouman TD (1991) J Phys Chem
112. Bak KL, Devlin FJ, Ashvar CS, Taylor PR, Frisch MJ, Stephens PJ (1995) J Phys Chem 99:14918
113. Bak KL, Jørgensen P, Helgaker T, Ruud K, Jensen HJAa (1994) J Chem Phys 100:6621
114. Bak KL, Jørgensen P, Helgaker T, Ruud K, Jensen HJAa (1993) J Chem Phys 98:8873
115. Cheesman JR, Frisch MJ, Devlin FJ, Stephens PJ (1996) Chem Phys Lett 252:211
116. Diem M (1993) Introduction to modern vibrational spectroscopy. Wiley, New York
117. Komornicki A, McIver JW (1979) J Chem Phys 70:2014
118. Amos RD (1986) Chem Phys Lett 124:376
119. Amos RD (1987) Molecular property derivatives. In: Lawly KP (ed) Ab initio methods in quantum chemistry. Wiley, New York, pp 99–153
120. Frish MJ, Yamaguchi Y, Gaw JF, Schaefer III HF, Binkley JS (1986) J Chem Phys 84:531
121. Johnson BG, Florian J (1995) Chem Phys Lett 247:120
122. Stirling A (1996) J Chem Phys 104:1254
123. Collier WB, Magdo I, Klots TD (1999) J Chem Phys 110:5710
124. Halls MD, Schlegel HB (1999) J Chem Phys 111:8819
125. van Caillie C, Amos RD (2000) Phys Chem Chem Phys 2:2123
126. Jürgensen VW, Jalkanen KJ (2006) Phys Biol 3:S63
127. Buckingham AD (1967) Adv Chem Phys 12:107
128. Atkins PW, Barron LD (1969) Mol Phys 16:453
129. Barron LD, Buckingham AD (1971) Mol Phys 20:1111
130. Fischer P, Hache F (2005) Chirality 17:421
131. Amos RD (1982) Chem Phys Lett 87:23
132. Helgaker T, Ruud K, Bak KL, Jørgensen P, Olsen J (1994) Faraday Discuss 99:165
133. Polavarapu PL (1990) J Phys Chem 94:8106
134. Barron LD, Gargaro AR, Hecht L, Polavarapu PL (1991) Spectrochim Acta A 47:1001
135. Barron LD, Gargaro AR, Hecht L, Polavarapu PL (1991) Spectrochim Acta A 48A:261
136. Barron LD (1982) Molecular light scattering and optical activity, 2nd edn. Cambridge University Press, Cambridge
137. Barron LD, Bogaard MP, Buckingham AD (1973) J Am Chem Soc 95:603
138. Hecht L, Barron LD (1990) Appl Spectrosc 44:483
139. Barron LD (2004) Molcular light scattering and optical activity 2nd edn. Cambridge University Press, Cambridge
140. Hecht L, Barron LD, Hug W (1989) Chem Phys Lett 158:341
141. Barron LD, Ford SJ, Bell AF, Wilson G, Hecht L, Cooper A (1994) Faraday Discuss 99:217
142. Yu G-S, Freedman TB, Nafie LA, Deng T, Polavarapu PL (1995) J Phys Chem 99:835
143. Kim J, Kapitan J, Lakhani A, Bour P, Keiderling TA (2007) Theor Chem Acc doi:10.1007/s00214-006-0183-4 (this issue)
144. Marinica DC, Grégoire G, Desfrançois C, Schermann JP, Borgis D, Gaigeot MP (2006) J Phys Chem A 110:8802
145. Devlin F, Stephens PJ (1987) Appl Spectrosc 41:1142
146. Diem M (1991) Vib Spectra Struct 19:1
147. Nafie LA (1997) Annu Rev Phys Chem 48:357
148. Nafie LA (1996) Appl Spectrosc 50:14A
149. Ellzy MW, Jensen JO, Hameka HF, Kay JG (2003) Spectrochim Acta A 59:2619
150. Cao X, Dukor RK, Nafie LA (2007) Theor Chem Acc doi:10.1007/ s00214-007-0284-8
151. Dukor RK, Nafie LA (2000) Vibrational optical activity of pharmaceuticals and biomolecules. In: Meyers RA (ed) Encyclopedia of analytical chemistry. Wiley, Hoboken, pp 662–676

152. Freedman TB, Cao X, Dukor RK, Nafie LA (2003) Chirality 15:743
153. Fristrup P, Lassen PR, Johannessen C, Tanner D, Norrby P-O, Jalkanen KJ, Hemmingsen L (2006) J Phys Chem A 110:9123
154. Fristrup P, Lassen PR, Tanner D, Jalkanen KJ (2007) Theor Chem Acc doi:10.1007/s00214-006-0186-1
155. Stephens PJ, Devlin FJ, Schürch S, Hulliger J (2007) Theor Chem Acc doi:10.1007/s00214-006-0245-7
156. Jalkanen KJ, Lassen PR, Hemmingsen L, Rodarte A, Degtyarenko IM, Nieminen RM, Christensen SB, Knapp-Mohammady M, Suhai S, Gale JD (2007) Theor Chem Account (this issue)
157. Bieri M, Gautier C, Bürgi (2007) Phys Chem Chem Phys 9:671
158. McDowell SAC, Buckingham AD (2007) Theor Chem Acc doi:10.1007/ s00214-006-0182-5
159. Nafie LA (1997) J Phys Chem A 101:7826
160. Hug W, Fedorovsky M (2007) Theor Chem Acc doi:10.1007/ s00214-006-0185-2
161. Jalkanen KJ, Gale JD, Jalkanen GJ, McIntosh D, El Azhary A, Keiderling TA, Jensen GM (2007) Theor Chem Account (this issue)
162. Jalkanen KJ, Stephens PJ (1991) J Phys Chem 95:5446
163. Parsons MT, Koga Y (2005) J Chem Phys 123:234504–1
164. Ramaekers R, Pajak J, Lambie B, Maes G (2004) J Chem Phys 120:4182
165. Marèchal Y (1996) Faraday Discuss 103:349
166. Wüthrich K, Billeter M, Güntert P, Luginhühl P, Riek R, Wider G (1996) Faraday Discuss 103:245
167. Barlow DJ, Thornton JM (1988) J Mol Biol 201:601
168. Baldwin RL (1989) Trends Biochem Sci 14:291
169. Deisenhofer J (2000) Mutat Res 460:143
170. Todo T (1999) Mutat Res 434:89
171. Berg BJV, Sancar GB (1998) J Biol Chem 273:20276
172. Langenbacher T, Zhao X, Bieser G, Heelis PF, Sancar A, Michel-Beyerle ME (1997) J Am Chem Soc 119:10532
173. Todo T, Takemori H, Ryo H, Ihara M, Matsunaga T, Nikaido O, Sato K, Normura T (1993) Naure 361:371
174. Cheam TC, Krimm S (1989) J Mol Struct (Theochem) 188:15
175. Balázs A (1990) J Phys Chem 90:2754
176. Cheam TC (1993) J Mol Struct 295:259
177. Beglov , Dmitrii , Roux , Benoit (1995) Biopolymers 35:171
178. Poon C-D, Samulski ET, Weise CF, Weisshaar JC (2000) J Am Chem Soc 122:5642
179. Weise CF, Weisshaar JC (2003) J Phys Chem B 107:3265
180. Nafie LA (2007) Theor Chem Acc doi:10.1007/s00214-007-0267-9
181. Lehmann MS, Koetzle TF, Hamilton WC (1972) J Am Chem Soc 94:2657
182. Diem M, Polavarapu PL, Oboodi M, Nafie LA (1982) J Am Chem Soc 104:3329
183. Diem M (1988) J Am Chem Soc 110:6967